processes

MDPI

Article

Preparation and Characterization of the Sulfur-Impregnated Natural Zeolite Clinoptilolite for Hg(II) Removal from Aqueous Solutions

Marin Ugrina [1,*], Martin Gaberšek [2], Aleksandra Daković [3] and Ivona Nuić [1]

[1] Department of Environmental Engineering, Faculty of Chemistry and Technology, University of Split, Ruđera Boškovića 35, 21 000 Split, Croatia; ivona@ktf-split.hr
[2] Department of Mineral Resources and Geochemistry, Geological Survey of Slovenia, Dimičeva Ulica 14, 1000 Ljubljana, Slovenia; martin.gabersek@geo-zs.si
[3] Institute for Technology of Nuclear and Other Mineral Raw Materials, P. O. Box 390, 11 000 Belgrade, Serbia; a.dakovic@itnms.ac.rs
* Correspondence: mugrin@ktf-split.hr; Tel.: +385-21-329-454

Abstract: Sulfur-impregnated zeolite has been obtained from the natural zeolite clinoptilolite by chemical modification with Na_2S at 150 °C. The purpose of zeolite impregnation was to enhance the sorption of Hg(II) from aqueous solutions. Chemical analysis, acid and basic properties determined by Bohem's method, chemical behavior at different pH_o values, zeta potential, cation-exchange capacity (CEC), specific surface area, X-ray powder diffraction (XRPD), scanning electron microscopy with energy-dispersive X-ray analysis (SEM-EDS), Fourier transform infrared spectroscopy (FTIR), as well as thermogravimetry with derivative thermogravimetry (TG-DTG) were used for detailed comparative mineralogical and physico-chemical characterization of natural and sulfur-impregnated zeolites. Results revealed that the surface of the natural zeolite was successfully impregnated with sulfur species in the form of FeS and CaS. Chemical modification caused an increase in basicity and the net negative surface charge due to an increase in oxygen-containing functional groups as well as a decrease in specific surface area and crystallinity due to the formation of sulfur-containing clusters at the zeolite surface. The sorption of Hg(II) species onto the sulfur-impregnated zeolite was affected by the pH, solid/liquid ratio, initial Hg(II) concentration, and contact time. The optimal sorption conditions were determined as pH 2, a solid/liquid ratio of 10 g/L, and a contact time of 800 min. The maximum obtained sorption capacity of the sulfur-impregnated zeolite toward Hg(II) was 1.02 mmol/g. The sorption mechanism of Hg(II) onto the sulfur-impregnated zeolite involves electrostatic attraction, ion exchange, and surface complexation, accompanied by co-precipitation of Hg(II) in the form of HgS. It was found that sulfur-impregnation enhanced the sorption of Hg(II) by 3.6 times compared to the natural zeolite. The leaching test indicated the retention of Hg(II) in the zeolite structure over a wide pH range, making this sulfur-impregnated sorbent a promising material for the remediation of a mercury-polluted environment.

Keywords: natural zeolite clinoptilolite; sulfur impregnation; chemical modification; mercury sorption; leaching

Citation: Ugrina, M.; Gaberšek, M.; Daković, A.; Nuić, I. Preparation and Characterization of the Sulfur-Impregnated Natural Zeolite Clinoptilolite for Hg(II) Removal from Aqueous Solutions. *Processes* **2021**, *9*, 217. https://doi.org/10.3390/pr9020217

Academic Editor: Claudia Belviso
Received: 30 December 2020
Accepted: 21 January 2021
Published: 25 January 2021

1. Introduction

Zeolites belong to the aluminosilicate group of minerals found in large quantities in nature, especially in volcanic sedimentary rocks, saline alkaline lakes and soils, deep marine sediments, and hydrothermal alternation systems. They are formed by the interaction of volcanic glass, ash, and water under different pressure and temperature conditions by complex multiphase reactions of dissolution and precipitation, most often under alkaline conditions [1,2]. Zeolites consisted of primary building units (PBUs), SiO_4 tetrahedrons. Interconnecting of PBUs via common oxygen atoms forms secondary building units (SBUs),

and their further crosslinking causes the formation of a three-dimensional zeolite crystal structure [3]. The spaces between the tetrahedrons are occupied by water molecules and consist of pores, channels, and cavities, creating the micro-, meso-, and macro-porous structure of a zeolite. The isomorphic substitution of tetravalent silicon with trivalent aluminum causes structural imperfection, generating a negative charge, which is compensated by electropositive hydrated alkali and alkaline earth cations [4–6]. Hydration of cations occurs due to the cationic electric field and the electric dipole moment of water. The presence of water in the structure allows cation mobility, whereby the cation–dipole interaction reduces the direct interaction of the zeolite lattice and the cations, which increases their mobility. Since the compensating cations are not structural components of zeolites, they are bound by weak Coulomb electrostatic interactions with a negatively charged lattice, which allows them to exchange with other ions, making zeolites ion exchangers [7–9]. Since natural zeolites are exploited from natural deposits, they represent low-cost and environmentally friendly sorbent materials in the field of green chemistry. Among all natural zeolites, clinoptilolite is the most widespread and most researched, and many studies have shown its effectiveness for heavy metals removal [10,11].

Among heavy metals, mercury is of particular concern due to its well-known toxicity to human health, high mobility, and tendency for bioaccumulation and biomagnification through the food chain [12]. Unfortunately, its extreme health toxicity and environmental problems are well known since the Minamata Bay accident in Japan [13]. Thus, the World Health Organization (WHO) and the US Environmental Protection Agency (USEPA) have introduced restrictions in the form of the maximum-permissible concentration of mercury in drinking water of up to 1 μg/L [14]. This value indicates the importance of mercury wastewater treatment as well as remediation of mercury-contaminated sites. Unlike controllable mercury-polluted wastewater, contaminated sites, especially near mercury mines, are of particular concern. Rainwater washes away the contaminated sites, and the mercury leachate percolates through the soil layers down to the groundwater, aquifer, and sediment. Therefore, it is of great interest to prevent the spread of contamination, most often by applying in situ remediation treatments such as placing a permeable reactive barrier or sprinkling the contaminated site with reactive material. In both cases, the reactive material should possess high efficiency for mercury immobilization and retention in its structure [15–17]. The key factor is the capacity of the sorbent to be implemented for remediation purposes. Different modifications of sorbents are performed in order to improve their sorption properties. Regarding mercury, its tendency to bind to sulfur species is well known, which leads to the formation of insoluble HgS [14,18]. Therefore, many studies have been conducted to impregnate the surface of sorbents with sulfur in order to improve their sorption capacity toward Hg(II). Various methods and chemicals are used, such as carbon disulfide (CS_2) [19–21], sodium sulfide (Na_2S) [22–26], potassium sulfide (K_2S) [18], sulfuric acid (H_2SO_4) [19,26], SO_2 [27,28], dimethyl disulfide (CH_3SSCH_3) [28], sulfur powder [28], and cystamine hydrochloride [29]. Chemical modification can lead to changes in sorbents' physico-chemical properties such as specific surface area, pore size, pore volume, functional groups, surface charge, and, finally, the mercury sorption capacity. These investigations have pointed out that sulfurization enhances the sorption ability of sorbents toward mercury. Based on the available literature, the most common sorbent for mercury immobilization is activated carbon [22,26–28,30], and activated carbon prepared from various organic waste materials [19,23,24].

In practical applications, each sorbent shows advantages and disadvantages. It is well known that synthetic materials, such as activated carbon, have a higher surface area compared to natural sorbents, such as zeolites, and therefore they are widely used in sorption processes. The limitations in the use of activated carbon as a sorbent for heavy metals lie in the fact that it is more effective for removing organic compounds. Therefore, in addition to the cost of activated carbon preparation, it is necessary to implement an appropriate treatment method for higher uptake of specific inorganic substances, which increases the total cost [31,32]. Unlike activated carbon, natural zeolites exhibit excellent

selectivity for heavy metal ions. Although they show a lower sorption capacity compared to synthetic sorbents, this limitation is compensated by their availability in large quantities worldwide, making them low-cost sorbents. To expand their applications, modified forms are used, while still retaining the name of inexpensive sorbents [3,10,11,33]. As we know to date, there is little available literature on the sulfurization of natural zeolites. Thus, the intention of this investigation was to expand the possibility of using natural zeolites for the remediation of a mercury-polluted environment. Based on the available literature, the modification method with Na_2S was chosen, since natural zeolites show a hydrophilic character and due to the simplicity of the procedure.

Therefore, the aim of this paper was the preparation of a sulfur-impregnated natural zeolite with Na_2S at 150 °C. Special attention was focused on the detailed mineralogical and physico-chemical characterization of the prepared sulfur-impregnated zeolite (SZ) compared to the starting material using methods for determining the acidity and basicity of the zeolite (Bohem's method), its chemical behavior at different pH_o values, zeta potential, as well as X-ray powder diffraction (XRPD), scanning electron microscopy with energy-dispersive X-ray analysis (SEM-EDS), FTIR, and thermogravimetry with derivative thermogravimetry (TG-DTG) techniques. Determination of optimal sorption conditions as well as the Hg(II) sorption mechanism onto the SZ sample was investigated. The results of this investigation should provide significant information about the possibility of using the prepared modified sorbent for remediation purposes.

2. Materials and Methods

2.1. Sorbent Preparation

The parent sample, a natural zeolite (NZ), was collected from the Zlatokop deposit (Vranjska Banja, Serbia). The sample was milled and sieved, and a particle size fraction of 0.6–0.8 mm was separated according to the standard method (DIN 66165-2) [34]. Thereafter, the sample was washed in ultrapure water and dried at 60 °C.

The chemical modification of NZ was based on several published methods [23–26,35]. Each method used Na_2S as a modification agent, while the process time, temperature, and concentration of Na_2S were different. Therefore, the optimal Na_2S concentration, time, and temperature were selected based on the preliminary investigations conducted. A mixture of 1 g of NZ and 10 mL of 1 mol/L Na_2S solution prepared from $Na_2S \times 9H_2O$ salt was refluxed for 4 h at 150 °C. After that, the sample was washed with ultrapure water until a negative reaction with sulfide ions occurred and a neutral pH was reached. Then, the sample was dried at 60 °C and stored in a desiccator until further use. The obtained sulfur-impregnated natural zeolite was marked as SZ.

2.2. Sorbent Characterization

The chemical composition of the parent zeolite and the sulfur-impregnated zeolite was determined by the classical chemical analysis of aluminosilicates [36].

The total acidity and total basicity of zeolites were determined by Bohem's titration method [37]. Acidic zeolite surface groups were determined by neutralization with excess NaOH and basic surface groups by neutralization with excess HCl. A mixture of 0.2 g of NZ or SZ with 20 mL of 0.1 mol/L standard NaOH (for determination of the acid group) or with 20 mL of 0.1 mol/L standard HCl (for determination of the basic group) solution was agitated for 24 h at 25 °C. Thereafter, the zeolite was separated from the liquid phase, and the unreacted NaOH was directly titrated with 0.1 mol/L of standard HCl solution, while unreacted HCl was directly titrated with 0.1 mol/L of standard NaOH solution. The amount of reacted NaOH represents the total amount of acidic surface groups, and the amount of reacted HCl represents the total amount of basic surface groups.

The chemical behavior of NZ and SZ samples was investigated in an aqueous solution of KNO_3 as a background electrolyte at 0.1 mol/L and 0.001 mol/L at different initial pH values (pH_o) in the range $2.04 < pH_o < 12.08$. The pH_o was adjusted by addition of 0.1 mol/L of KOH or HNO_3. Then, 0.1 g of each sample was mixed with 50 mL of the pre-

pared solution with different pH_o values for 24 h at room temperature. After equilibration, the suspensions were filtered and equilibrium pH (pH_e) values were measured.

The zeta potential of NZ and SZ samples was determined using Zetasizer Nano ZS90 (Malvern Instruments, Malvern, UK) in distilled water at pH 5.82. Solutions of testing materials (0.5 mg/mL) were dispersed, and an average of 5 measurements was taken to represent the measured potential. Latex dispersion supplied by the instrument manufacturer was used as a calibration standard.

The cation-exchange capacity (CEC) of NZ and SZ samples was measured by standard US EPA SW-846 Method 9080 (1 mol/L of sodium acetate, pH 7) [38]. The CEC value determined was 1.42 meq/g for NZ and 2.61 meq/g for SZ.

The specific surface area (SSA) was determined using the Brunauer, Emmet, and Teller (BET) method by nitrogen adsorption. Samples were degassed for 24 h at 130 °C in Flow-Prep 060 Degasser, and the SSA was measured by a Micrometrics Gemini 2360 Analyzer. The Barrett, Joyner, and Halenda (BJH) method was used for calculating the pore volume and pore radius.

X-ray powder diffraction (XRPD) analysis was used to determine the phase composition of NZ and SZ samples. Samples were analyzed on a Phillips PW-1710 X-ray diffractometer with a curved graphite monochromator and a scintillation counter. The intensities of diffracted CuKα X-ray radiation (λ = 1.54178 Å) were measured at room temperature in the range from 4° to 65° 2θ, with a step scan of 0.02 °2θ and a time of 1 s.

The morphology as well as qualitative and semi-quantitative chemical composition of the surface of NZ and SZ samples were analyzed using scanning electron microscopy (SEM) with energy-dispersive X-ray spectroscopy (EDS). The SEM-EDS analysis was performed using JEOL JSM 6490LV SEM coupled with an Oxford INCA EDS system, consisting of an Oxford INCA PentaFET3 Si(Li) detector and INCA Energy 350 processing software. The samples were carbon-coated before the analysis to obtain their conductivity. The analysis was done in high vacuum at a 20 kV accelerating voltage, a spot size of 28 or 50, a working distance of 10 mm, and an EDS acquisition time of 60 s. Secondary electron (SE) mode was used to study the morphological characteristics of the samples' surface, and backscattered electron (BSE) mode was used to distinguish newly formed Hg phases from the surface of zeolite particles, since Hg phases are brighter than zeolites in BSE mode.

The surface of the NZ and SZ samples was also analyzed with a MXFMS-BD optical microscope (Ningbo Sunny Instruments Co) at a magnification of 50× and photographed with a digital camera.

Fourier transform infrared spectroscopy (FTIR) analysis of NZ and SZ samples was performed on a Thermo Nicolet FTIR 6500 spectrometer in transmission mode. Samples were prepared by the KBr pellets method, and spectra were recorded in the wavelength range of 4000–500 cm^{-1} at a resolution of 0.48 cm^{-1}.

Thermal analysis of NZ and SZ samples was performed using Perkin Elmer STA 6000. Samples were heated from 40 C to 1000 °C in a nitrogen atmosphere at aheating rate of 10 °C/min.

2.3. Batch Sorption Experiment

All chemicals used, $Hg(NO_3)_2 \cdot H_2O$ and 0.1 mol/L and 1 mol/L of HNO_3, were of analytical grade. A stock solution of 14.099 mmol/L of Hg(II) was prepared from the salt of $Hg(NO_3)_2 \cdot H_2O$ by dissolving it in ultrapure water. Solutions of lower concentrations were prepared by diluting the stock solution in ultrapure water. The pH of the prepared Hg(II) solutions was adjusted by adding a few drops of 0.1 mol/L or 1 mol/L of HNO_3. All experiments were performed in batch mode using an incubator shaker, within 24 h, at 230 rpm and 25 °C. The initial and equilibrium Hg(II) concentrations were determined by using Flame Atomic Absorption Spectrophotometer PinAAcle 900F (AAS), and the pH_e was also measured.

The effect of the pH_o of Hg(II) solutions (pH_o = 2.09 and 2.30) was determined based on a relatively low pH precipitation limit. The 1.0 g of NZ or SZ was agitated with 100 mL of the 4.193 mmol Hg/L solution.

The effect of the solid/liquid (S/L) ratio was carried out at optimal pH_o (=1.98) determined on the basis of a previous experiment. A different mass of SZ in the range of 0.2–1.4 g (S/L ratio = 2, 6, 10, and 14 g/L) was mixed with 100 mL of the 4.193 mmol Hg/L solution.

The effect of the initial concentration, 0.461–14.099 mmol Hg/L, at optimal pH_o, $1.99 < pH_o < 2.10$, as well as at an optimal S/L ratio determined on the basis of a previous experiment, was examined by mixing 1.0 g of SZ with 100 mL of Hg(II) solution. In addition, in all supernatants, the concentration of released exchangeable Na^+, K^+, Ca^{2+}, and Mg^{2+} was determined using ion chromatography (Metrohm 761 Compact IC).

The effect of the contact time was carried out at optimal conditions of pH_o 1.98, S/L ratio of 10 g/L, and initial concentration of 10.146 mmol Hg/L, where the maximum sorption capacity of SZ was observed. The 20.0 g of SZ was agitated with 2 L of Hg(II) solution, and 10 mL of samples were taken at desired time intervals within 24 h. The total sampling volume was less than 5–6% of the total solution volume. The mercury-saturated sample was washed several times in ultrapure water, dried at 40 °C, and marked as SZHg. SZHg was characterized by SEM-EDS and TG-DTG analyses, as well as leaching properties in ultrapure water at different pH_o values were estimated. For comparison, TG-DTG analysis of a Hg(II)-saturated NZ sample was also performed.

In all experiments conducted, sulfide leaching was not observed by a qualitative method [39].

The amount of Hg(II) sorbed onto the zeolite in time t, q_t (mmol/g), as well as the removal efficiency in time t expressed as a percentage, α_t (%), were calculated by Equations (1) and (2) [18,40]:

$$q_t = (c_o - c_t) \cdot \frac{V}{m}, \quad (1)$$

$$\alpha_t = \frac{(c_o - c_t)}{c_o} \cdot 100, \quad (2)$$

where c_o and c_t are the concentrations of Hg(II) at t = 0 and time t (mmol/L), V is the volume of the solution (L), and m is the mass of the zeolite (g). If time t is equal to 24 h, then q_t and α_t have equilibrium values, q_e and α_e.

2.4. Leaching Experiments

The leaching of sorbed Hg(II) from the collected saturated SZHg sample was examined according to the standard leaching method (DIN 38414 S4) in ultrapure water at a pH_o range of 2.04–12.13 [41]. The mass of 1.0 g of SZHg was mixed with 10 mL of ultrapure water with different pH_o values for 24 h at 25 rpm and 25 °C. After 24 h, suspensions were filtered, and the concentration of leached Hg(II) was determined in supernatants by using an AAS, as well by determination of pH_e values.

The amount of Hg(II) leached from SZHg, q_{leach} (mmol/g), and the percentage of Hg(II) leached from SZHg, α_{leach} (%), were calculated according to Equations (3) and (4) [18,40]:

$$q_{leach} = c_{leach} \cdot \frac{V}{m}, \quad (3)$$

$$\alpha_{leach} = \frac{q_{leach}}{q_e} \cdot 100, \quad (4)$$

where c_{leach} is the concentration of the Hg(II) leached from the saturated zeolite (mmol/L).

3. Results and Discussion

3.1. Mineralogical and Physico-Chemical Characterization of Sorbents

The chemical composition of the natural zeolite (NZ) and the sulfur-impregnated zeolite (SZ) is summarized in Table 1, while the calculated element quantities based on the chemical composition are shown in Table 2.

Table 1. Chemical composition of natural zeolite (NZ) and sulfur-impregnated zeolite (SZ).

Sample	Content, wt %										
	SiO_2	Al_2O_3	Fe_2O_3	Na_2O	K_2O	CaO	MgO	TiO_2	S	SO_3	Loss of Ignition
NZ	66.56	13.41	1.95	1.56	1.12	4.00	0.54	0.169	0.16	0.40	10.24
SZ	56.69	12.34	2.07	10.70	0.76	4.03	0.73	0.168	1.08	2.70	9.76

Table 2. Element quantity of NZ and SZ.

Sample	Element Quantity, mmol/g										
	Na	K	Ca	Mg	Al	Si	O	Fe	Ti	S	Si/Al
NZ	0.503	0.238	0.713	0.134	2.630	11.077	27.80	0.244	0.021	0.100	4.21
SZ	3.454	0.161	0.719	0.181	2.420	9.435	26.14	0.259	0.021	0.674	3.89

Results showed that sulfur modification caused an increase in the quantity of sodium and sulfur as well as a decrease in the silicon content, while the quantity of other constituents changed negligibly. It is interesting to note that the quantity of calcium remained unchanged after sulfur modification. Among exchangeable cations, calcium dominates in the NZ and sodium in the SZ sample. The modification also caused a decrease in the Si/Al ratio, indicating that desilication takes place during treatment of the zeolite with Na_2S. A significant increase in the quantity of both sulfur and sodium by about 6.8 times indicated that chemical modification of the zeolite surface with Na_2S was successful.

The acidic or basic properties of zeolites are extremely important as they affect the charge of the zeolite surface, depending on the pH value of the surrounding medium, and thus significantly affect the zeolite sorption properties. The charge properties of NZ and SZ were estimated by determining the amount of total acidic and total basic sites, the chemical behavior at different pH_o values, and the zeta potential. These parameters are listed in Table 3 for both NZ and SZ.

Table 3. Total acidic and basic surface sites and zeta potential of NZ and SZ.

Sample	Total Acidic Sites (meq/L)	Total Basic Sites (meq/L)	Zeta Potential (pH = 5.82)
NZ	46.3	30.0	−22.8
SZ	2.5	190.0	−39.9

Results showed that NZ possesses more acidic than basic sites, determined according to Bohem's method. Sulfur modification caused a drastic decrease in acidity and an increase in basicity of the SZ sample. In general, the increase in the basic properties of zeolites can be achieved by reducing the Si/Al ratio and increasing the electropositive counterbalancing extra-framework zeolite cations, most often alkaline cations. This can be accomplished by treating the zeolite in an alkaline medium, whereby the desilication of the zeolite structure occurs [4]. The results of the element quantity for NZ and SZ (Table 2) confirmed that treatment with Na_2S caused a decrease in the Si/Al ratio. The presence of a high amount of OH^- causes hydrolysis of the aluminosilicate structure, resulting in relatively easy cleavage of the Si–O–Si bond compared to the Si–Al–O bond [4,5]. Therefore, the amount of aluminum does not change, which is not the case in an acidic medium when dealumination

is pronounced. It is known that aluminum in the $[AlO_4]^{5-}$ tetrahedral structure is the carrier of the negative charge of the zeolite lattice. However, extraction of only one silicon atom from an orthosilicate anion $[SiO_4]^{4-}$ causes the formation of four unpaired oxygen atoms, which bring a negative charge and additionally increase the negative charge of the lattice. Thus, unpaired oxygen atoms act as Lewis bases and possess significant basicity, and their charge is compensated by sodium ions that act as Lewis acids [4]. Figure 1 shows a schematic representation of the possible configuration of the zeolite framework after desilication [4,5].

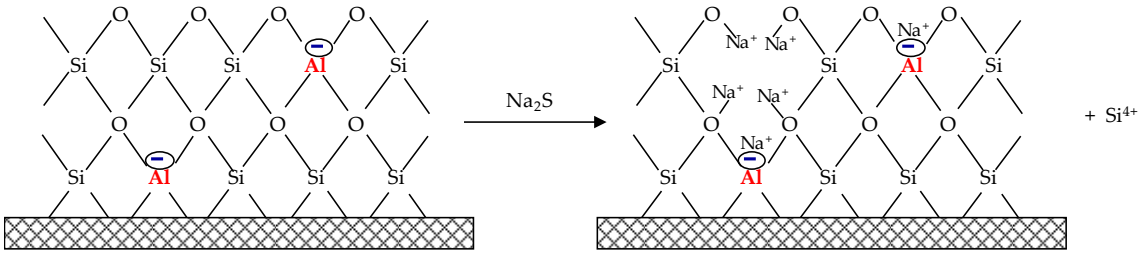

Figure 1. Schematic representation of zeolite configuration after silicon dissolution in a strong alkaline medium.

Since it was found that sulfur modification caused an increase in basicity and thus an increase in the net negative zeolite charge, the chemical behavior of NZ and SZ was estimated from the dependence of pH_e on different pH_o values at the two ionic strengths of the electrolyte (Figure 2).

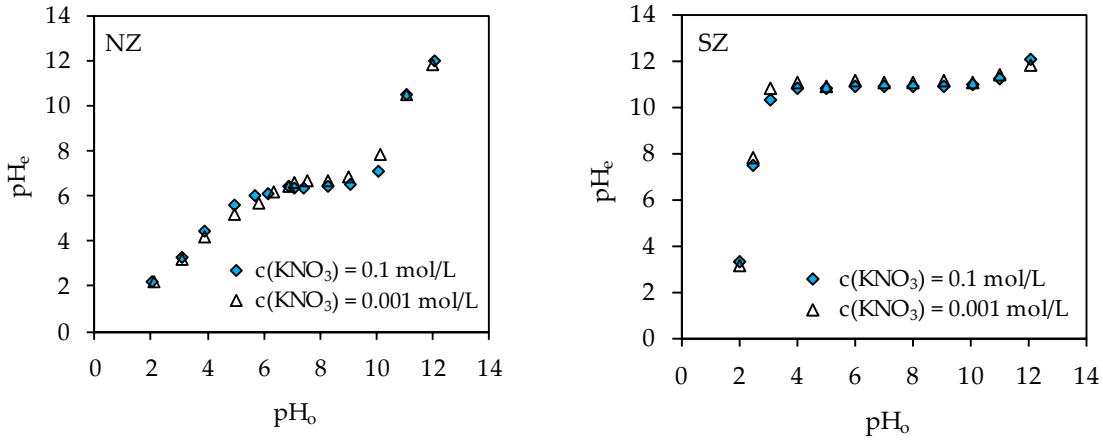

Figure 2. pH_e vs. pH_o in a suspension of NZ (left) or SZ (right) and an electrolyte solution of different ionic strengths.

The results showed an increase in pH_e in the range of pH_o = 2–9 for NZ, i.e., in the range of pH_o = 2–10 for SZ. In contrast, at pH_o > 9 for NZ and pH_o > 10 for SZ, a decrease in pH_e relative to pH_o was observed. This indicated that the zeolite surface possesses functional groups that are protonated in an acidic medium and deprotonated in an alkaline medium according to the following reactions [42]:

$$\equiv T - OH + H^+ \rightarrow \equiv T - OH_2^+, \quad (5)$$

$$\equiv T - OH + OH^- \rightarrow T - O^- + H_2O, \quad (6)$$

where T is Si or Al.

The change in the pH_e of the surrounding medium in the above-mentioned wide pH range shows the buffering properties of SZ due to the negative charge of the lattice. It can be seen from Figure 2 that a plateau is broader for SZ (3–10) in comparison to NZ (6–9) and for four pH units higher, indicating a higher affinity of SZ toward H^+ ions due to ahigher net negative charge. Thus, the increase in pH_e is due to neutralization of the

negative charge of the zeolite lattice as a consequence of sulfur modification. An increase in the negative charge is also supported by the results of the measured zeta potentials for NZ and SZ in distilled water at pH = 5.82 (Table 3), which indicate that both zeolites at pH = 5.82 still have a negative charge, which corresponds to the plateau of the curve in Figure 2. At aforementioned conditions, SZ has almost twice more net negative charges than NZ. The plateau is established due to the low concentration of H^+ ions, which are not sufficient to fully compensate the negative charge of the zeolite lattice. Furthermore, at the inflection point, pH $\leq$ 3 for SZ and pH $\leq$ 6 for NZ, the charge of the zeolite particles could change from negative to positive due to the large amount of available H^+ ions that cause protonation of zeolite active groups. Thus, results showed that both NZ and SZ have a net negative charge, and in contact with a solution of a high concentration of H^+ ions, it probably becomes positive. Therefore, an increase in the negative charge of SZ could enhance the sorption capacity toward positive Hg(II) species due to electrostatic attraction with a negative zeolite surface.

The specific surface area (SSA), pore volume, and pore radius of NZ and SZ are listed in Table 4.

Table 4. The specific surface area, pore volume, and pore radius of NZ and SZ.

Sample	Specific Surface Area (m^2/g)	Pore Volume (cm^3/g)	Pore Radius (nm)
NZ	19.447	0.082	1.979
SZ	12.064	0.081	1.953

Results revealed that the SSA of SZ was significantly reduced compared to NZ. An increase in the SSA was expected, since desilication of the zeolite was confirmed. Therefore, the decrease in the SSA confirms the deposition of sulfur at the zeolite surface, which blocks available pores and thus reduces the SSA. Yuan et al. reported that sulfur impregnation of powdered activated carbon with different concentrations of Na_2S significantly decreases the SSA as the sulfur content in impregnated activated carbon increases [24]. Silva et al. investigated the modification of activated carbon obtained from eucalyptus wood with carbon disulfide, and a decrease in the SSA was observed due to pore blocking with surface-sulfurized groups [19]. The aforementioned observations are in agreement with our results. A slight decrease in the total pore volume and pore radius was also observed, whereby simultaneous desilication and sulfide deposition probably had a negligible effect on the change in the pore volume and pore radius.

X-ray powder diffraction (XRPD) analysis of the NZ and SZ samples is shown in Figure 3.

From Figure 3, it is evident that both samples have the same crystal composition. This indicates that modification with sulfur did not cause changes in the mineral composition. The most represented component is the heulandite type of the zeolite clinoptilolite, while quartz, feldspars, and clay minerals are much rarer. Regarding feldspar minerals, plagioclases prevail over K-feldspars. A decrease in the peaks' intensity is observed on the X-ray powder diffractogram of the SZ sample compared to NZ. This can be attributed to a decrease in crystallinity due to sulfur modification that causes desilication of the zeolite particle, which is confirmed by a decrease in the Si/Al ratio (Table 2) as well as sulfur deposition on the zeolite surface, probably in amorphous form. Since sulfur is probably deposited in amorphous form, characteristic peaks were not observed on the diffractogram.

EDS analysis of the NZ and SZ surface was done on eight fields per sample at a magnification of 35× (Figure 4). The corresponding elemental composition of the analyzed fields (given in wt %) is listed in Tables 5 and 6.

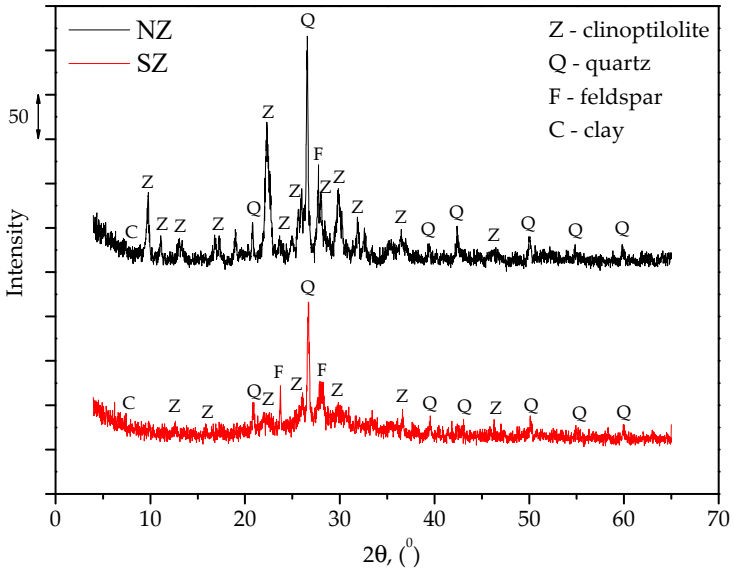

Figure 3. XRPD spectra for NZ and SZ.

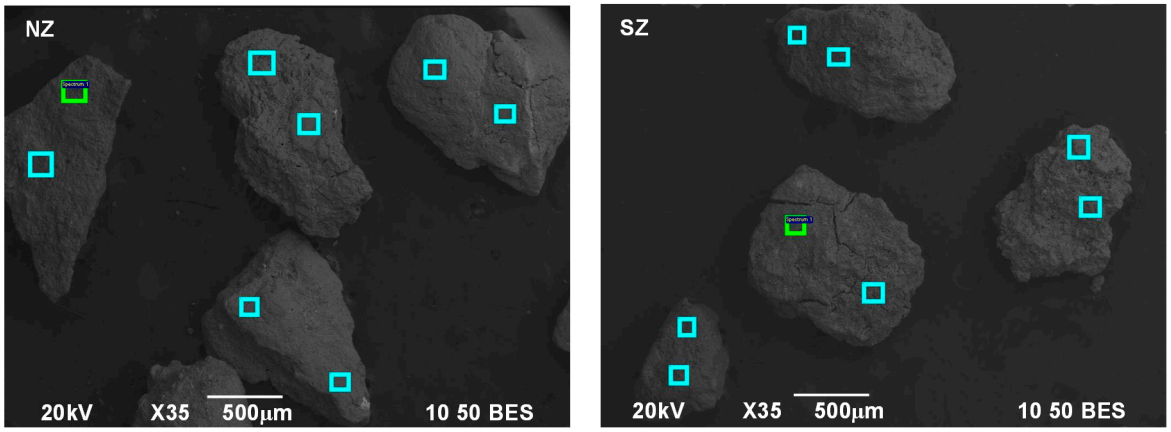

Figure 4. Backscattered electron mode (BSE) images of NZ (left) and SZ (right) with marked eight fields (spectra, Sp) per sample for EDS analysis.

Table 5. Semi-quantitative chemical composition (given in wt %) of the eight analyzed fields on the NZ sample (spectra, Sp; analyzed with EDS).

Element	O	Na	Mg	Al	Si	K	Ca	Fe
Sp 1	59.10	0.37	0.77	6.02	30.50	1.02	2.22	-
Sp 2	59.36	0.56	0.72	6.01	30.00	0.97	2.09	0.29
Sp 3	52.77	0.76	0.47	5.79	35.48	1.38	2.74	0.60
Sp 4	55.67	0.74	0.61	5.89	32.99	1.34	2.77	-
Sp 5	58.61	0.38	2.01	8.37	23.37	3.65	0.48	2.59
Sp 6	58.14	0.41	2.11	8.35	23.44	3.46	0.53	3.11
Sp 7	52.91	0.45	0.64	5.89	32.40	1.25	3.00	3.46
Sp 8	45.00	-	0.55	6.05	33.17	1.76	4.42	7.50
Mean	55.20	0.46	0.99	6.55	30.17	1.85	2.28	2.19

Table 6. Semi-quantitative chemical composition (given in wt %) of the eight analyzed fields on the SZ sample (spectra, Sp; analyzed with EDS).

Element	O	Na	Mg	Al	Si	S	K	Ca	Fe
Sp 1	56.59	16.11	-	6.51	15.80	1.43	0.33	0.80	2.43
Sp 2	56.15	14.36	0.34	7.34	17.50	1.03	0.41	1.58	1.29
Sp 3	56.32	13.21	0.50	6.62	18.68	1.02	0.43	2.12	1.10
Sp 4	55.03	15.18	-	7.66	16.25	1.80	0.38	0.47	3.22
Sp 5	55.97	15.22	-	8.30	17.86	1.20	0.22	0.40	0.83
Sp 6	57.11	16.45	-	7.77	16.64	1.13	0.34	-	0.56
Sp 7	59.64	19.55	-	5.46	12.25	1.36	0.23	0.91	0.61
Sp 8	59.78	18.34	0.30	5.94	12.50	1.42	0.25	1.03	0.44
Mean	57.07	16.05	0.14	6.95	15.94	1.30	0.32	0.91	1.31

Based on the results shown in Tables 5 and 6, a mostly uniform elemental composition was observed on all spectra for both NZ and SZ. Comparing the mean mass percentage values of detected elements on the NZ and SZ surface, the values of oxygen and aluminum were almost identical, the values of iron and silicon decreased by two times, while the value of sodium increased by even 35 times as a result of the modification with Na_2S. The uniform distribution of sulfur on all marked fields of SZ is worth noting. This indicates the fine distribution of sulfur on the zeolite surface, confirming impregnation of the zeolite surface with sulfur. It was observed that during modification in the alkaline medium, desilication occurred, i.e., breaking of Si–O chains. This caused an increase in the negative charge of the zeolite structure, which was neutralized by sodium ions. The values of other alkaline and alkaline earth cations (K, Mg, Ca) are lower for SZ than for NZ since during treatment with Na_2S, in addition to neutralization of the negative charges by sodium ions, the ion exchange of K, Mg, and Ca with Na also takes place.

To detect the main mineral component, clinoptilolite, a SEM image of both samples at a magnification of 10,000× was taken (Figure 5).

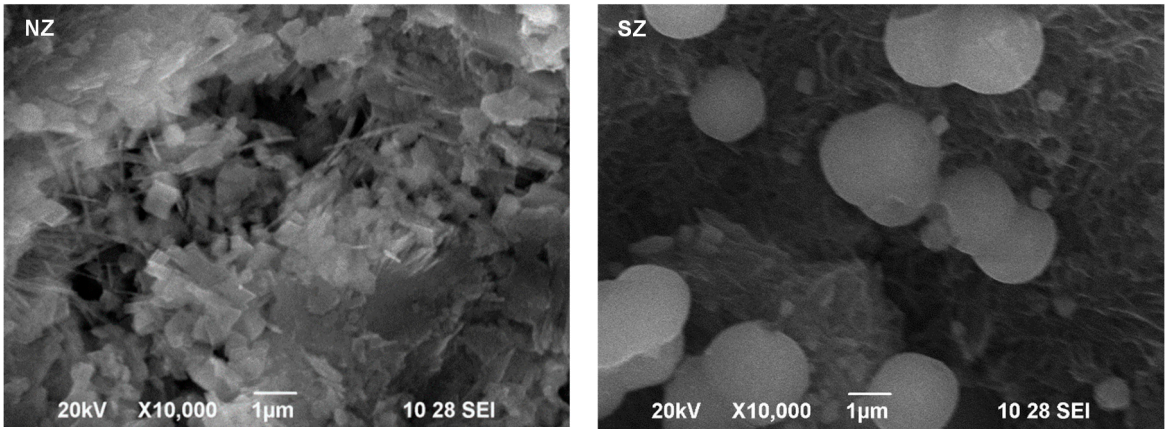

Figure 5. SEM secondary electron image of NZ (**left**) and SZ (**right**) at a magnification of 10,000×.

The characteristic plate structure for clinoptilolite can be seen in the SEM images of NZ. At the same magnification, mostly regular spherical clusters were observed on the surface of SZ. An additional SEM image (Figure S1) of the SZ sample at a magnification of 600× showed a clear change in surface morphology. Thus, the surface coverage is evident, which is the reason why clinoptilolite platelets are not visible in Figure 5 (right). This is also supported by a decrease in the SSA (Table 4).

To determine the composition of the observed clusters on the surface of the SZ sample, another SEM image was taken at a magnification of 5000×. EDS analysis of three selected points, two inside the cluster and one outside, was performed (Figure 6), and the mass percentage of the detected elements is presented in Table 7.

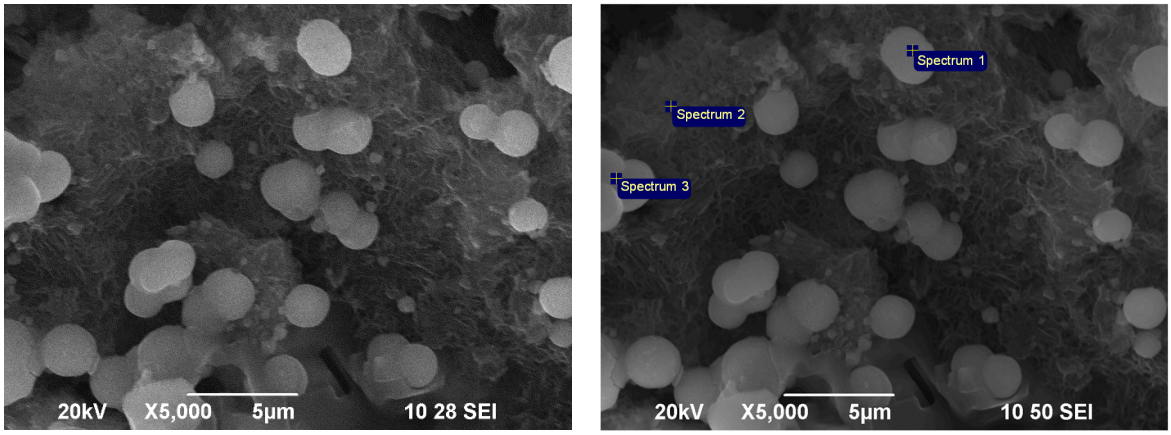

Figure 6. SEM secondary electron image of SZ (**left**) and corresponding SEM secondary electron image with three marked points for EDS analysis (**right**), both at a magnification of 5000×.

Table 7. Semi-quantitative chemical composition (given in wt %) of spherical clusters (Sp 1, Sp 3) and the surface of SZ (Sp 2).

Element	O	Na	Mg	Al	Si	S	K	Ca	Fe
Sp 1	50.85	6.67	1.10	4.43	24.68	3.32	1.11	2.49	5.35
Sp 2	58.98	8.71	0.70	7.00	20.11	1.36	0.34	1.88	0.93
Sp 3	49.02	8.07	0.50	8.44	25.67	2.03	0.70	2.75	2.83

The results shown in Table 7 confirmed that the observed clusters (Sp 1 and 3) contain a higher amount of sulfur compared to the surrounding area without clusters. Higher values of calcium and iron were also observed in spectra 1 and 3 belonging to the clusters, while the values of other elements were very similar for all three spectra. According to this, sulfur deposition is higher at sites with higher amounts of iron and calcium. It could be assumed that the formed clusters could be sulfides of calcium and iron. Taking into account the amount of calcium and iron (Table 2), probably both sulfides are formed where CaS should be present in a higher amount. Also, the eventually formed Fe_2S_3 is unstable and decomposes to FeS and elemental sulfur at temperatures above 20 °C [43]. Since the color of the zeolite sample changed after sulfur impregnation, both samples were photographed before and after impregnation (Figure 7).

(**a**) (**b**)

Figure 7. Photographs of (**a**) NZ and (**b**) SZ samples.

Figure 7 clearly shows that the zeolite particles were coated with a black film attributed to iron sulfide species, since all iron sulfides are known to be black in color. However, it can be noticed that the black color on the zeolite particles is not uniform and contains white dots. Therefore, NZ and SZ were compared by optical microscopy at a magnification of 50× and are shown in Figure 8.

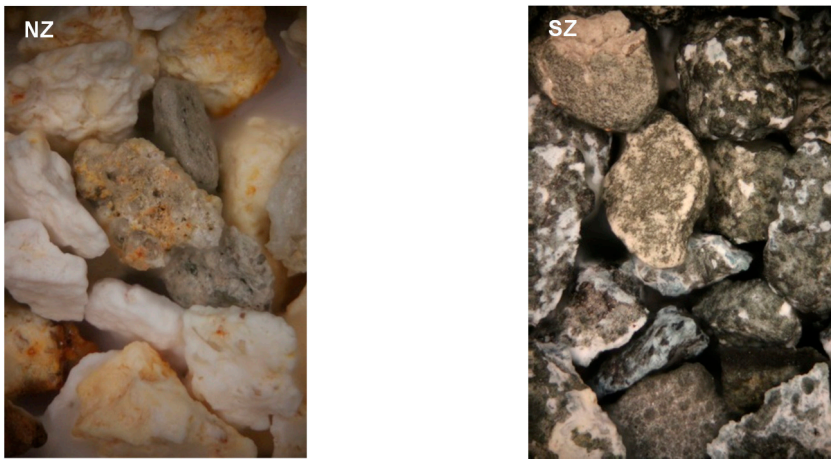

(**a**) (**b**)

Figure 8. Optical micrographs of the (**a**) NZ and (**b**) SZ surface at a magnification of 50×.

It was observed that NZ has a light color characteristic of aluminosilicate minerals. Yellow stains could also be observed on the particles, which can be attributed to the iron content in NZ. Contrary to NZ, black and white spots were observed on SZ. Since CaS is white in color, white spots could be attributed to its formation on the surface of zeolite particles. Namely, due to the huge amount of sodium from Na_2S, sodium ions are exchanged with calcium ions, which are probably trapped on the surface of the zeolite in the form of CaS, at a high concentration of sulfide ions.

FTIR analysis of NZ and SZ was performed in order to obtain information about zeolite functional groups. The FTIR spectra of both samples are depicted in Figure 9.

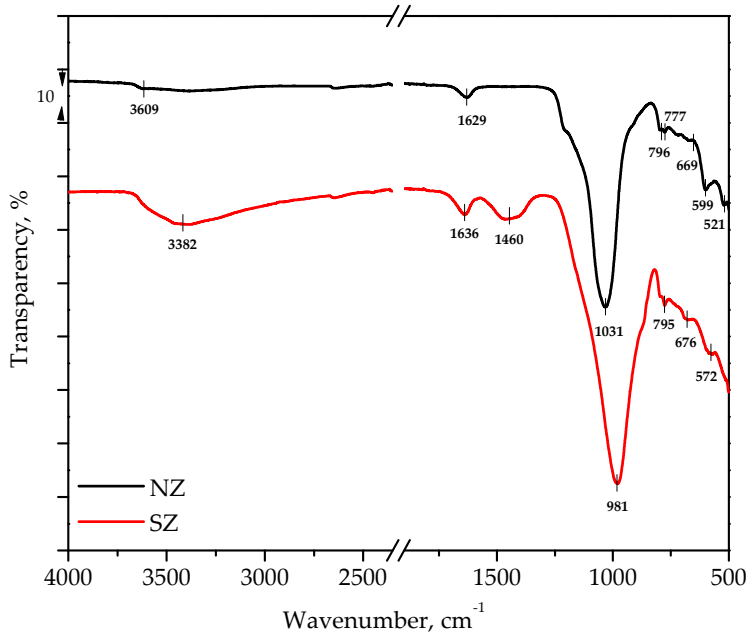

Figure 9. FTIR spectra of NZ and SZ.

The FTIR spectra of NZ and SZ samples were quite similar and showed the characteristic bands for aluminosilicate minerals marked in Figure 9. Results indicated that sulfur impregnation did not change characteristic spectral zeolite band vibrations, while visible differences were observed in the sulfur-impregnated sample, showing broad bands with a higher intensity (3382 cm^{-1}) as well as the appearance of a new band at 1460 cm^{-1}. The band with a shoulder at 3609 cm^{-1} for NZ was assigned to the vibration of the hydroxyl groups (O–H stretching) [44]. For SZ, a broad band was observed in the range of 3700–2800 cm^{-1}, with a shoulder at 3382 cm^{-1}. The extension of this band could be ascribed to the vibration of the hydroxyl groups, with the basic properties confirming their presence in SZ. Cadiș et al. in their investigation provided information about the FTIR spectra of Na_2S [45]. They found a characteristic broad band in the range of 3600–2500 cm^{-1}, with a shoulder at 3372 cm^{-1}, which they assigned to O–H stretching of adsorbed water on the surface of Na_2S. Therefore, this confirms the deposition of Na_2S on the surface of the sulfur-impregnated zeolite, which is consistent with SEM-EDS analysis and a decrease in the SSA. A zeolite water-bending vibration (O–H) at 1629 and 1636 cm^{-1} confirms the presence of zeolite water [44]. The presence of a pronounced band with a shoulder at 1460 cm^{-1} only for SZ indicates that this peak could be attributed to a newly formed group due to zeolite sulfur modification. The presence of sulfur in the form of a thiol group does not correspond to this band, since the thiol group shows vibration at 2800 cm^{-1} [46]. Also, iron sulfide species show characteristic bands at wavelengths below 600 cm^{-1}, which cannot be detected due to overlapping with spectral zeolite banding vibration as well as probably low amounts of iron in the zeolite compared to Si, Al, and O [47,48]. According to Song et al., this band could be attributed to the CaS formed during modification treatment [49]. The strongest vibration band at 1031 and 981 cm^{-1} belongs to the asymmetric Si–O or Al–O stretching vibration in the Si or Al tetrahedral structure. The bands in the range of 700–500 cm^{-1} correspond to pseudo-lattice vibrations, symmetry O–Al–O or O–Si–O stretching [50].

Investigation of sample mass change as a function of temperature can be very useful since it can indicate changes in the physical and chemical properties of a sample. Thermal analysis of NZ and SZ was performed, and the curves of mass change as a function of temperature (TG) as well as the curve of mass rate change as a function of temperature (DTG) are shown in Figure 10.

The TG-DTG curves of NZ showed that mass loss occurred in three steps. The first mass loss (60–150 °C) is attributed to the loss of weakly bound water, the second one (150–250 °C) is due to the loss of bound water to exchangeable cations, and the least pronounced, last one (450–500 °C) corresponds to the loss of structurally bound water [51]. In the case of the SZ sample, three mass losses were also observed. Major decomposition occurred at 60–250 °C, corresponding to the elimination of both weakly bound water and water coordinated to exchangeable cations. Compared to NZ, which showed two mass losses in the temperature range of 60–250 °C, the SZ sample show only one, probably due to the high amount of exchangeable Na ions as a consequence of the modification. The second mass loss (300–380 °C) probably corresponds to the dehydroxylation and decomposition of the sulfides formed on the surface of the zeolite during the modification. The SZ sample showed a higher total mass loss (14.42%) compared to the NZ sample (12.72%), which is attributed to the higher amount of sodium and thus the higher hydration of the zeolite.

3.2. Determination of Optimal Mercury Sorption Parameters

The influence of pH, S/L ratio, contact time, and initial concentration on the sorption efficiency and amount of sorbed Hg(II) onto the SZ sample was examined. It is extremely important to optimize all the above parameters in order to determine the concentration range in which the sorbent shows the maximum efficiency with a minimum mass of sorbent used and at a minimum contact time. Since pH directly affects the surface charge of the sorbent, as well as the type of Hg(II) species, the effect of pH on the sorption efficiency of Hg(II) onto SZ was first examined and compared to NZ.

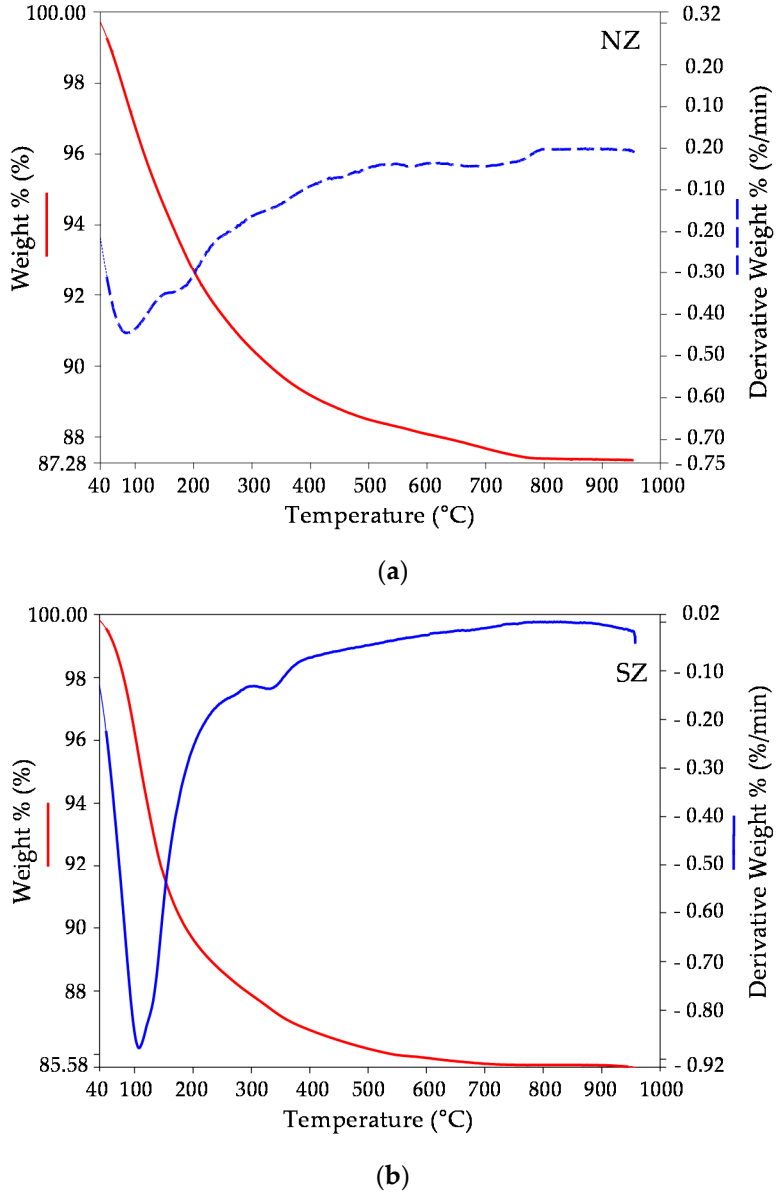

Figure 10. TG-DTG curves for (**a**) NZ and (**b**) SZ.

According to the Hg(II) distribution diagram at different pH values shown in Figure S2, Hg^{2+} species exist as dominant ones up to pH = 2.9, $HgOH^{+}$ appears in the range 1.5 < pH < 4.5 with a maximum proportion at pH = 3.0, while the precipitation of mercury in the form of hydroxide begins at pH > 2.4, and above pH = 4.7, mercury is present only as $Hg(OH)_2$ [52]. It can be seen from this that it is very important to conduct the experiment under conditions where the precipitation of mercury in solution will not be possible. Therefore, for all performed experiments, the pH values at which the precipitation of Hg(II) will occur (pH_{ppt}) depending on the initial Hg(II) concentration in the solution were calculated according to Equation (7) [42]:

$$pH_{ppt} = 14 - \log\sqrt{\frac{c_o(Hg^{2+})}{K_{sp}[Hg(OH)_2]}}, \quad (7)$$

where $c_o(Hg^{2+})$ is the initial concentration of Hg(II) and K_{sp} is the solubility product constant of $Hg(OH)_2$ ($K_{sp}[Hg(OH)_2] = 3.9 \cdot 10^{-26}$) [53].

Figure 11a shows the changes in pH_e values, depending on the pH_o for NZ and SZ, as well as the calculated pH_{ppt} value for a given initial concentration of 4.193 mmol Hg/L, while Figure 11b shows the Hg(II) removal efficiency for the two pH_o values for NZ and SZ.

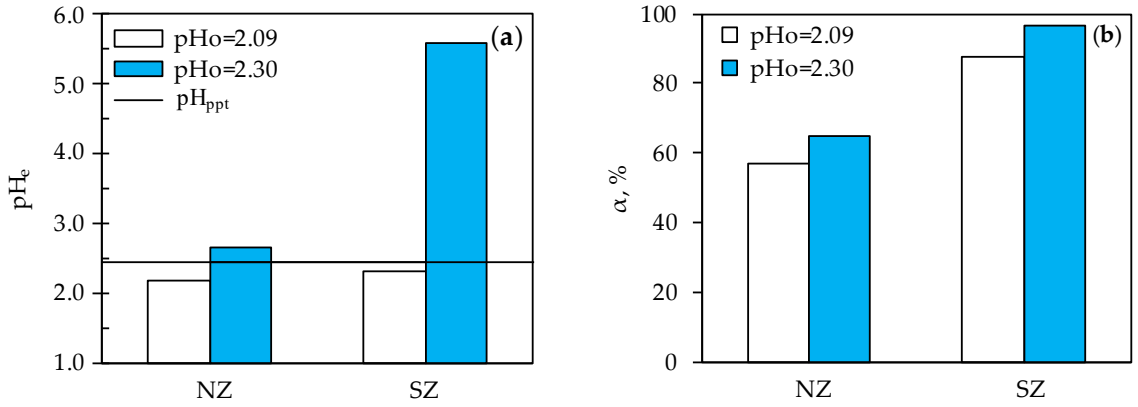

Figure 11. (**a**) pH_{ppt} and pH_e after sorption of Hg(II) onto NZ and SZ at pH_o = 2.09 and 2.30. (**b**) Removal efficiency of Hg(II) for NZ and SZ at pH_o = 2.09 and 2.30.

A narrow pH range was chosen in order to avoid mercury precipitation as well as dissolution of the zeolite structure, which occurs below pH 2. From Figure 11a, it can be seen that at pH_o = 2.30, $pH_e > pH_{ppt}$, indicating that precipitation of Hg(II) occurs in the solution for both sorbents. Since $pH_e < pH_{ppt}$ at pH_o = 2.09, precipitation does not occur, indicating that pH_o = 2.09 represents the optimal pH for Hg(II) sorption onto both NZ and SZ. Comparing the Hg(II) removal efficiency onto NZ (56.94%) and SZ (87.84%) at pH_o = 2.09 (Figure 11b), it is noticed that the modification contributes to an increase in the α value by 1.5 times under given experimental conditions. The removal efficiency at pH_o = 2.30 was not taken into account since it was the result of not only Hg(II) sorption but also precipitation.

The effect of the S/L ratio was examined at optimal pH = 2.09 and the same initial concentration of 4.193 mmol Hg/L. The results of the amount of sorbed Hg(II) per gram of SZ as a function of the S/L ratio are shown in Figure 12a. Figure 12b shows a comparison of pH_o, pH_e, and pH_{ppt} values as a function of the S/L ratio.

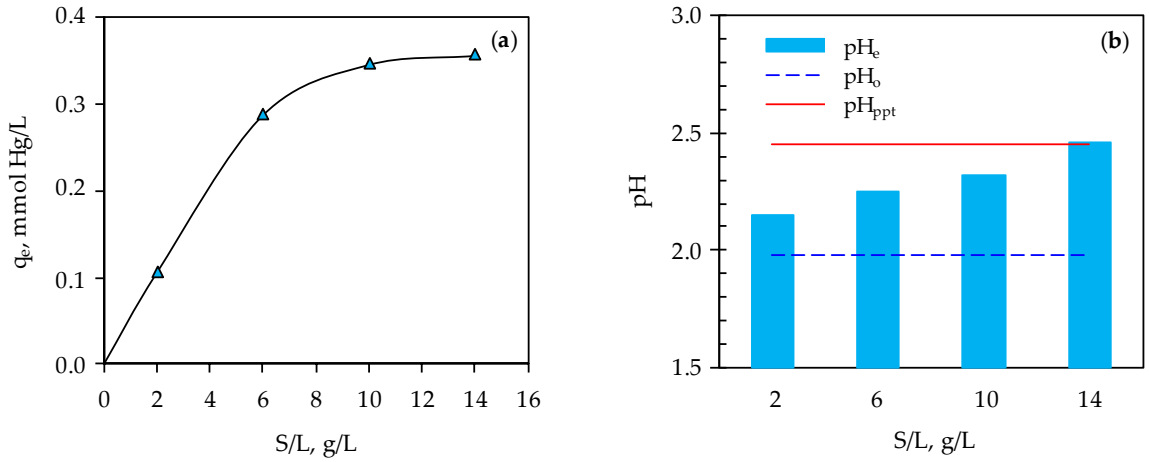

Figure 12. (**a**) The effect of the solid/liquid (S/L) ratio on the amount of Hg(II) sorbed onto SZ. (**b**) Comparison of pH_e and pH_{ppt} with pH_o in relation to the S/L ratio.

The amount of sorbed Hg(II) increased with an increasing S/L ratio up to 10 g/L, after which q_e achieved a constant value (Figure 12a). The increase in the amount of Hg(II)

sorbed with an increase in the S/L ratio is attributed to the higher amount of available active sites. Since the c_o of Hg(II) is constant, an increase in the S/L ratio affects the increase in q_e to a critical value, which in our case is 10 g/L, where the achieved q_e value is 0.35 mmol Hg/g. However, the results shown in Figure 12b also serve to determine the optimal S/L ratio. For S/L ratio = 2, 6, and 10 g/L, $pH_e < pH_{ppt}$, while for S/L ratio = 14 g/L, pH_e slightly exceeds the calculated pH_{ppt} value, which indicate that S/L ratio = 10 g/L is optimal. The increase in pH is due to the negative charge that is neutralized by H^+ ions, indicating that at low pH, competition between H^+ ions and Hg(II) species could be expected. This confirms that determining the optimal S/L ratio is also crucial to avoid Hg(II) precipitation in solution, since an increase in the S/L ratio results in an increase in pH_e.

The effect of the contact time on the change in q_t and α_t values is shown in Figure 13.

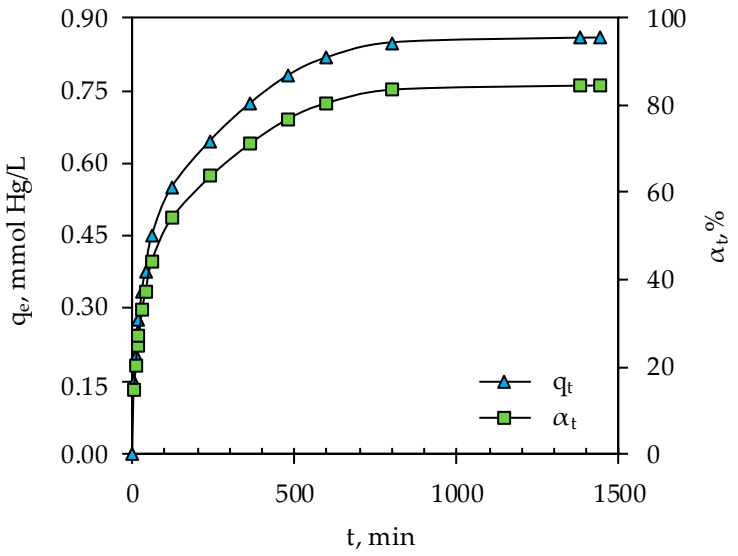

Figure 13. The quantity of Hg(II) removed per gram of SZ and removal efficiency in relation to contact time.

It was observed that the removal efficiency increased sharply in the first 120 min of the experiment, achieving an efficiency of 54%. Thereafter, the α_t value increased until equilibrium was established, which happened after 800 min, where α_t equaled 84.50%. Thus, it is observed that the sorption kinetics of Hg(II) takes place in two stages: the fast stage, in which the majority of Hg(II) is sorbed at easily available sites, most probably the surface-active sites, followed by the slow stage, in which the zeolite gradually saturates, in which Hg(II) is sorbed on less available sites, in pores and cavities inside the zeolite particle. At equilibrium, an amount of sorbed Hg(II) of 0.86 mmol/g was achieved.

The effect of the initial concentration on the amount of sorbed Hg(II) onto SZ as well as on the removal efficiency was examined and is shown in Figure 14.

Results showed a linear increase in the amount of sorbed Hg(II), with an increase in the initial concentration up to c_o = 12.26 mmol Hg/L, after which a plateau was established. At c_o > 12.26 mmol Hg/L, all available sorption sites are saturated, and each subsequent increase in c_o will not affect the increase in the q_e value. In contrast, the removal efficiency of Hg(II) decreases with an increase in the initial concentration. However, it is worth noting that for c_o < 8.29 mmol Hg/L, an efficiency higher than 92.28% is achieved. This indicates that the sulfur-impregnated zeolite shows excellent sorption ability toward Hg(II) over a wide concentration range. The maximum amount of sorbed Hg(II) onto SZ was 1.02 mmol Hg/g, which is 3.6 times higher than that for NZ, whose maximum sorbed amount was 0.28 mmol Hg/g [40]. The obtained results showed a significant increase in the amount of sorbed Hg(II), making the sulfur-impregnated zeolite a promising sorbent for application in the remediation of a mercury-polluted environment. This is supported

by the fact that in real conditions, where the concentration of mercury might be lower than 0.46 mmol/L, SZ could be used for remediation purposes, since an efficiency of 96% was achieved for the lowest tested concentration of 0.46 mmol Hg/L.

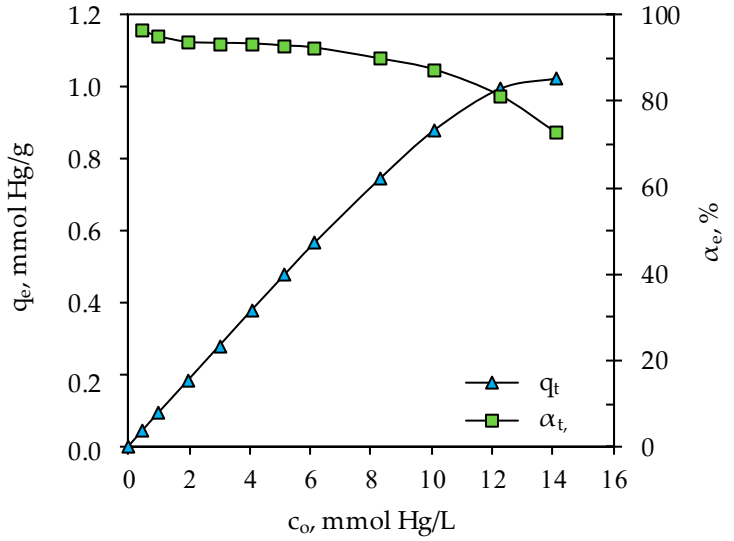

Figure 14. Amount of sorbed Hg(II) and removal efficiency in relation to the initial Hg(II) concentration.

Figure 15 shows the relationship between the amount of sorbed Hg(II) and the released exchangeable zeolite cations (Na, K, Ca, and Mg) and pH_e as a function of the initial Hg(II) concentration.

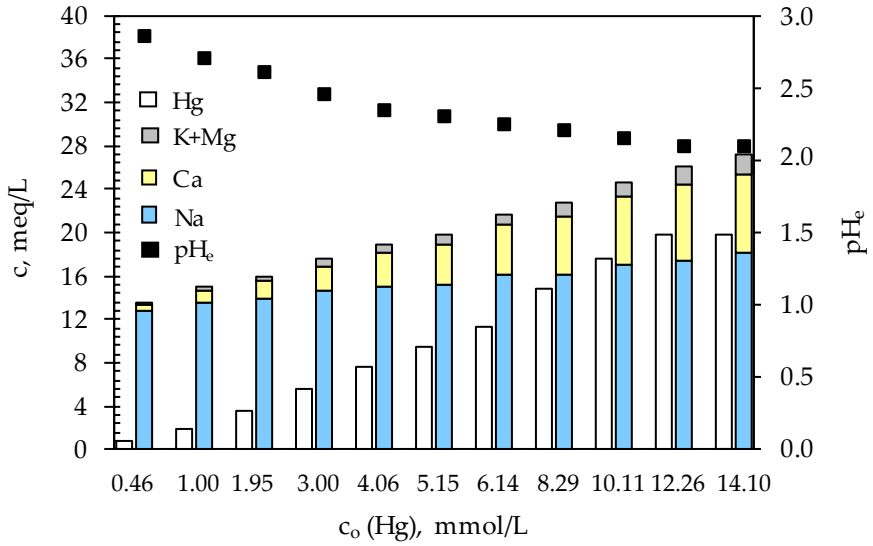

Figure 15. Relationship between the amount of sorbed Hg(II) and the released exchangeable zeolite cations and pH_e as a function of the initial Hg(II) concentration.

Results showed a nonstoichiometric relationship between the amount of sorbed Hg(II) and the released exchangeable ions. However, an increase in the amount of sorbed Hg(II) is accompanied by an increase in the amount of released exchangeable cations, suggesting that ion exchange could be the main mechanism of Hg(II) sorption onto zeolites. This is supported by the fact that the difference between the amount of Hg(II) sorbed and the amount of the released exchangeable cations decreases with increasing initial Hg(II) concentration. This also indicates the competition between Hg(II) and H^+ ions due to the high concentration of H^+ ions ($1.99 < pH_o < 2.10$) in initial Hg(II) solutions. The competition

effect is more pronounced at the lowest Hg(II) concentrations since the negative charge of SZ is compensated by electrostatic attraction of both H^+ ions and Hg(II) species. The competition effect weakens with an increase in the initial Hg(II) concentration, which is also confirmed by monitoring of pH_e values. A smaller increase in pH_e compared to pH_o ($1.99 < pH_o < 2.10$) was observed with an increase in the initial concentration of mercury, i.e., the amount of Hg(II) sorbed, where all pH_e values were less than the calculated pH_{ppt} values.

Confirmation of the competition effect is also provided by the determined CEC value of the SZ sample (2.61 meq/g), according to which the maximum amount of Hg(II) sorbed per gram of SZ should be 1.31 mmol/g, which is higher than the experimentally obtained capacity of 1.02 mmol Hg(II) per gram of SZ, indicating that complete saturation of SZ with Hg(II) was not achieved.

The dominant exchangeable cation in SZ is sodium (Figure 15), which was also confirmed by chemical analysis and SEM-EDS analysis of SZ. It is also observed that with an increase in c_o(Hg), the amount of released sodium increases slightly, while released calcium ions are more pronounced. The reason for this could be the partial dissolution in an acidic medium of the eventually formed CaS during the modification process, since the solubility product constant of CaS ($K_{sp} = 6.3 \cdot 10^{-8}$) is less than eventually formed FeS ($K_{sp} = 6.3 \cdot 10^{-19}$) [53]. Accordingly, Ca ion exchange with Hg(II) forms hard soluble HgS ($K_{sp} = 3.9 \cdot 10^{-53}$) [54]. Therefore, the SEM-EDS analysis of the mercury-saturated SZ could provide insight into the mechanism of Hg(II) sorption.

3.3. Characterization of the Mercury-Saturated Sulfur-Impregnated Zeolite

EDS analysis of the SZ surface after saturation with Hg(II) (sample name SZHg) was done on eight fields at a magnification of 35× (Figure 16). The corresponding elemental composition of the analyzed fields (given in wt %) is presented in Table 8.

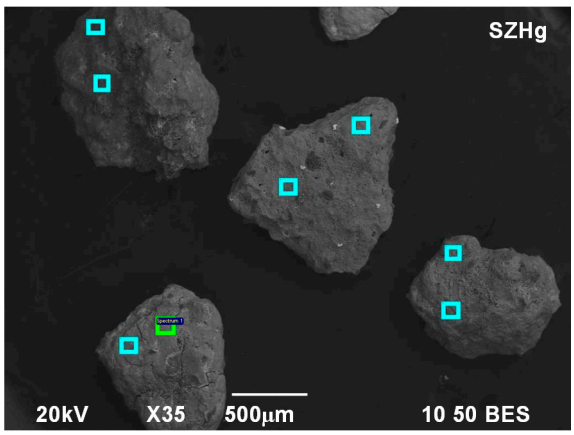

Figure 16. Backscattered electron mode (BSE) images of SZHg with marked eight fields (spectra, Sp) for EDS analysis.

Results confirmed the presence of Hg(II) in all eight observed fields, but with Hg(II) accumulation in higher quantities in some places compared to the others. Comparing the mean mass percentage values of the detected elements on the marked fields of SZ (Table 6) and SZHg (Table 8) samples, the values of sodium decreased drastically, while the values of sulfur and iron changed slightly as other detected elements. This indicates that sodium is exchanged with Hg(II) species and H^+ ions, which is in agreement with the results of monitoring the amount of released exchangeable cations during the sorption process. However, since it was difficult to connect the higher Hg(II) values with the content of sulfur on individual marked fields, an additional SEM-EDS analysis was performed at a higher magnification of 1000×. The BSE image of the four marked fields is shown in Figure 17 and the results of the elements detected by EDS analysis in Table 9.

Table 8. Semi-quantitative chemical composition (given in wt%) of the eight analyzed fields on the SZHg sample (spectra, Sp; analyzed with EDS).

Element	O	Na	Mg	Al	Si	S	K	Ca	Fe	Hg
Sp 1	34.75	1.60	-	6.75	16.03	1.07	-	0.34	-	39.46
Sp 2	38.09	2.36	-	7.18	14.57	1.27	0.39	0.39	-	35.75
Sp 3	42.84	0.48	0.58	4.09	25.85	0.63	0.37	0.70	-	24.46
Sp 4	41.20	0.37	0.51	4.07	24.14	1.12	0.41	0.52	0.49	27.17
Sp 5	45.83	0.40	0.83	4.08	17.43	1.60	0.37	0.43	4.53	24.49
Sp 6	50.44	0.61	0.89	4.17	22.22	0.82	0.93	0.60	4.59	14.73
Sp 7	43.81	-	0.28	4.84	22.75	1.02	0.86	0.43	2.83	23.20
Sp 8	45.98	-	0.32	4.85	20.26	0.58	0.53	0.34	2.03	25.10
Mean	42.87	0.73	0.43	5.00	20.63	1.01	0.48	0.47	1.81	26.80

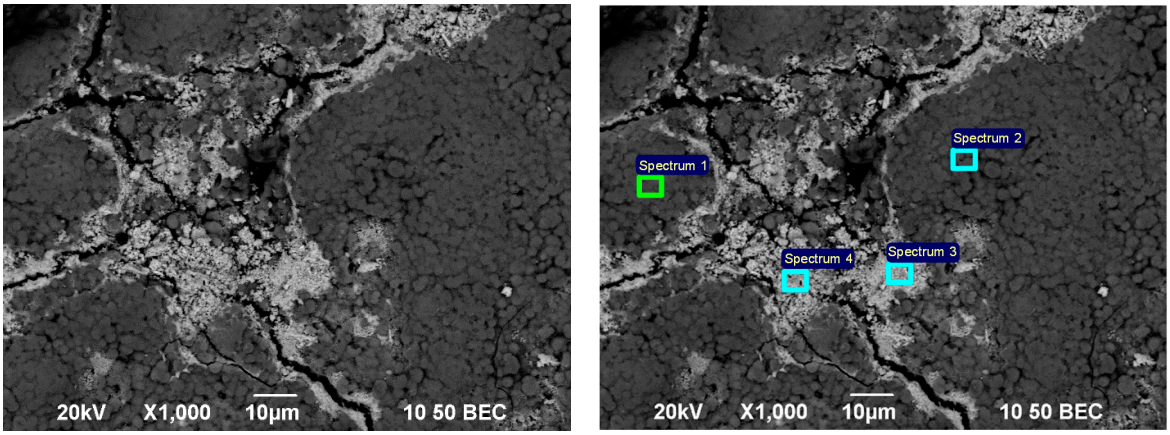

Figure 17. Backscattered electron mode (BSE) image of SZHg (**left**) and the corresponding BSE image with marked four fields (spectra, Sp) for EDS analysis (**right**), both at a magnification of 1000×.

Table 9. Semi-quantitative chemical composition (given in wt %) of the four analyzed fields on the SZHg sample (spectra, Sp; analyzed with EDS).

Element	O	Na	Al	Si	S	Ca	Fe	Hg
Sp 1	35.69	1.21	7.95	15.95	-	0.29	-	38.92
Sp 2	39.44	1.35	8.43	16.78	-	0.26	0.41	33.32
Sp 3	9.00	-	0.52	1.53	11.50	-	1.10	76.34
Sp 4	10.97	-	0.48	1.52	10.56	-	3.35	73.12

The BSE image shows unevenly distributed bright agglomerates indicating the formation of a new phase on the sample surface. Therefore, two fields outside (Sp 1 and 2) and two inside (Sp 3 and 4) the agglomerates were analyzed. The results showed a two times' higher amount of Hg(II) on the observed agglomerates. Areas where there are no agglomerates mainly contain Hg(II) and oxygen, while agglomerates primarily contain Hg(II) and sulfur. This indicates that a higher amount of sorbed Hg(II) may be associated with higher amounts of sulfur on the surface of SZ, where higher amounts of iron were also observed. Thus, more intensive sulfurization of the zeolite surface could be associated with a higher iron content, and the results of SEM-EDS, FTIR, and TG-DTG of SZ analysis confirmed the formation of both CaS and FeS on the surface of the zeolite after modification. However, since calcium was not recorded in spectra 3 and 4, it could be concluded that

higher amounts of Hg(II) are connected with the dissolution of the CaS formed, where free sulfide ions and Hg(II) species form less soluble HgS on the SZ surface. This is supported by an increase in the amount of released calcium ions with an increase in the amount of sorbed Hg(II) (Figure 15). Thus, these results show that Hg(II) is sorbed over the entire surface of the SZ sample, while sites a with higher sulfur content show higher affinity for Hg(II) species.

The TG-DTG curves for Hg(II)-saturated NZ and SZ are shown in Figure 18.

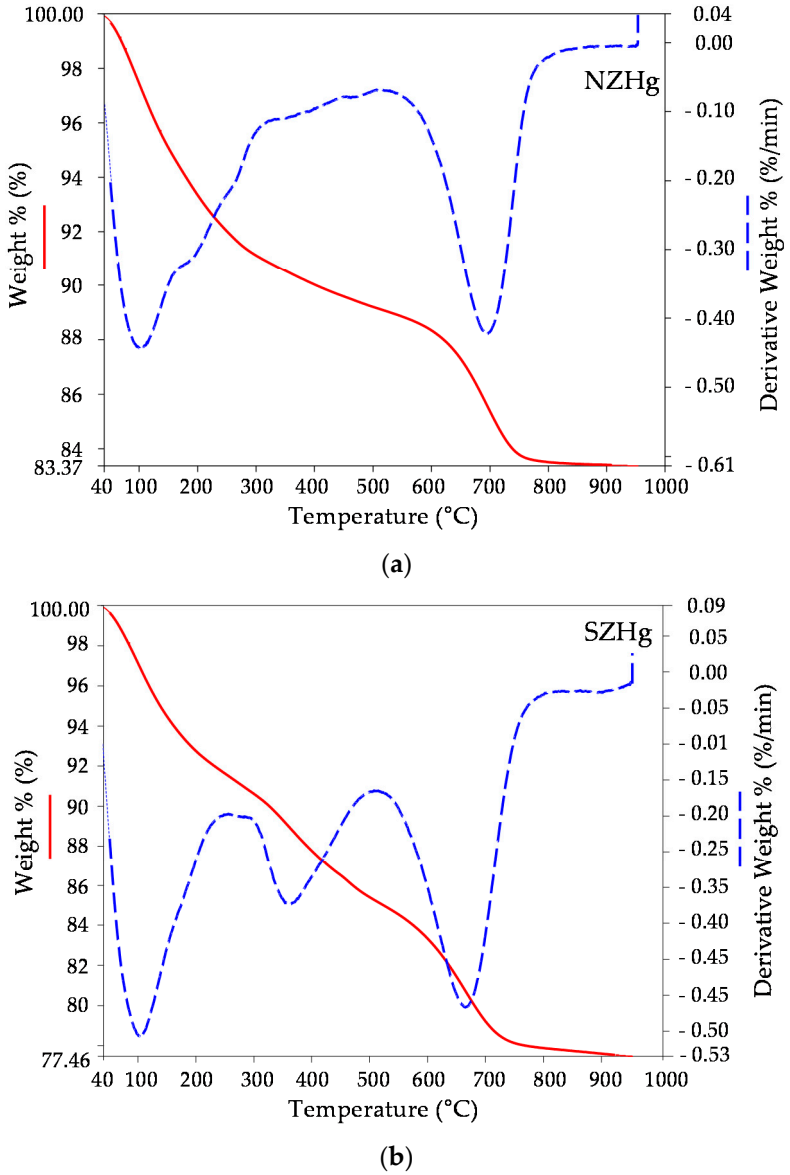

Figure 18. TG-DTG curves for **(a)** NZHg and (**b**) SZHg.

It can be observed that both saturated samples show similar mass loss in the same temperature range up to 300 °C. Above 300 °C, the significant mass loss at 600–800 °C for NZHg can be attributed to dehydroxylation and volatilization of mercury complexes. Praus et al., who investigated the sorption of Hg(II) onto montmorillonite, also observed mass loss at 550–800 °C in TG curves, which they attributed to mercury complexes on the montmorillonite surface [55]. On the other hand, Brigatti et al. [56] had the same observations for Hg(II) sorption studies on montmorillonite, which they attributed to the volatilization of mercury species as well as the intercalation of Hg–O species. The SZHg sample shows the existence of two mass losses at temperatures above 300 °C. Mass loss

in the range of 300–500 °C is ascribed to HgS decomposition. These observations are consistent with the study of Rumayor et al., who reported the thermal decomposition of HgS in one step, with a shoulder peak at 305 °C [57]. Further mass loss occurring in the temperature range of 550–800 °C corresponds to decomposition of sorbed Hg(II) species. The total mass loss of saturated SZHg (22.54%) is higher compared to NZHg (16.63%), which is related to a higher affinity of SZ than NZ for Hg(II). TG-DTG analysis in combination with SEM-EDS analysis confirmed that a significantly higher capacity of the SZ toward Hg(II) compared to NZ was due to the impregnation of the surface with sulfur.

Taking into account all the obtained results, the removal of Hg(II) species by SZ is a complex process and involves several possible sorption mechanisms. The increase in basicity and thus the negative surface charge causes electrostatic attraction of Hg(II) species; ion exchange of Hg(II) species with exchangeable zeolite cations, among which sodium dominates; and surface complexation on the oxygen-containing surface group and FeS, accompanied by co-precipitation on the SZ surface in the form of HgS due to partial dissolution of CaS. The sorption mechanism of Hg(II) species onto SZ is illustrated in Figure 19 [58,59].

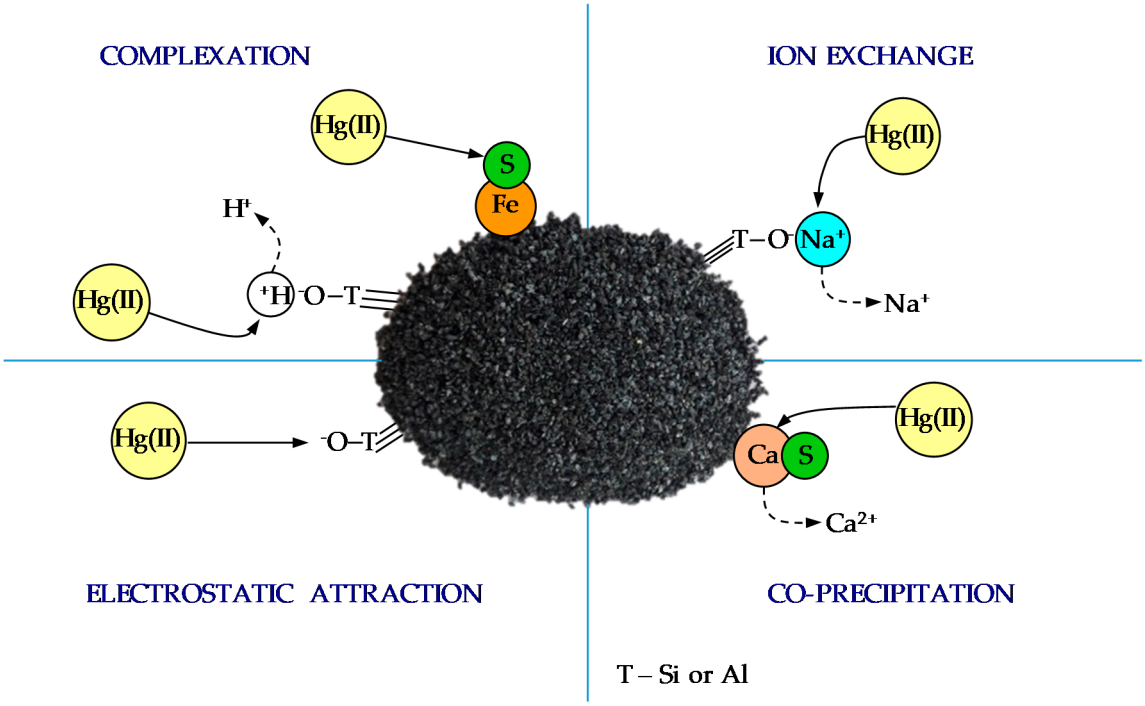

Figure 19. Illustration of proposed sorption mechanism of Hg(II) species onto SZ.

3.4. Leaching Properties of the Mercury-Saturated Sulfur-Impregnated Zeolite

Leaching properties of the mercury-saturated sulfur-impregnated zeolite, SZHg, was conducted in ultrapure water at a pH range of 2.00–12.05 according to the standard leaching method (DIN 38414) [41]. The purpose of the leaching test was to elucidate the strength of Hg(II) sorption onto SZ in order to determine its possible application for in situ remediation of a mercury-polluted environment. The results of the leaching test are shown in Figure 20.

It can be seen that in the pH range $4.02 \leq pH_o \leq 10.02$, Hg(II) leaching occurs only up to 0.3%. These results confirm that in a wide pH range, SZ has the ability to retain sorbed Hg(II) in its structure. In the extremely acidic, $pH_o \leq 3.05$, or alkaline, $pH_o \geq 11.02$, medium, a slight leaching of Hg(II) up to 4.1% was observed. Since the results of SEM-EDS and TG-DTG analyses of saturated samples confirmed different mechanisms of mercury sorption, in the form of HgS and ≡S–OHg, this indicates that these species sorbed with different strengths onto SZ. The interaction of the oxygen atom from the hydroxyl group with

Hg(II) is much weaker compared to the strong binding of Hg(II) to the sulfur-containing group [14]. Therefore, the cleavage of the Hg–O bond is more pronounced with increasing concentration of H^+ ions, leading to a higher percentage of leached Hg(II) from the SZHg sample. In an alkaline medium, less leaching could be expected due to the possible formation of insoluble $Hg(OH)_2$. However, in an extremely alkaline medium, desilication of the zeolite structure occurs, resulting in leaching of Hg(II). From Figure 20, it can be seen that at $pH_o > 7.02$, pH_e values decrease, especially at $pH_o > 11.02$. This also confirms the hydroxylation of the zeolite surface, which causes the cleavage of Si–O bonds. Thus, in the wide pH range that can be expected under real conditions, the SZ sample firmly sorbs Hg(II) in its structure as a result of sulfurization of the zeolite surface. This suggests that a sulfur-impregnated zeolite could have potential application as a material for in situ remediation of a mercury-polluted environment.

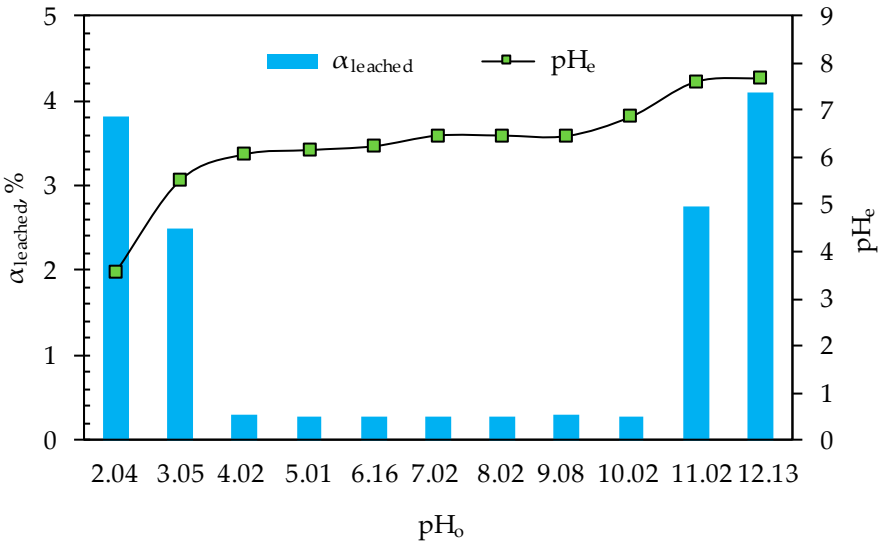

Figure 20. Percentage of leached Hg(II) from saturated SZHg and pH_e as a function of ultrapure water at different pH_o values.

From an environmental point of view, it is important to consider how to manage with a mercury-saturated zeolite. In the case of wastewater treatment in an industrial plant, the regeneration of zeolites would be the most acceptable solution with the reuse the regenerate in an industrial process. In contrast, by applying a zeolite for in situ remediation of mercury-contaminated sites, since it shows a low degree of mercury leaching, the saturated zeolite could be stabilized/solidified into building materials and used for fills and embankment, especially in road construction [60–62].

4. Conclusions

The sulfur-impregnated natural zeolite clinoptilolite was successfully prepared for Hg(II) removal from aqueous solutions. Detailed mineralogical and physico-chemical characterization of natural and sulfur-impregnated zeolites was explained. SEM-EDS analysis indicated a fine distribution of sulfur over the entire surface of the chemically modified zeolite, which confirms its impregnation. The increase in the amount of sulfur on the surface of the modified sample was associated with sites of higher calcium and iron content. The sulfur modification resulted in the formation of clusters that are attributed to CaS and FeS compounds. The possibility of the formation of these compounds was confirmed by SEM-EDS, FTIR, and TG-DTG analyses. A decrease in the specific surface area of the impregnated sample was observed, which is evidence of the deposition of sulfur species that blocked the pores on the zeolite surface. Chemical modification with Na_2S caused desilication of the zeolite structure, which was confirmed by chemical analysis,

i.e., by a decrease in the Si/Al ratio. Desilication caused a decrease in crystallinity (XRPD) and an increase in basicity, i.e., an increase in the content of oxygen-containing active groups. This caused an increase in the negative charge, which was compensated by the presence of exchangeable sodium ions. Optimal conditions for the implementation of sorption of Hg(II) species on the sulfur-impregnated zeolite were defined: pH = 2, S/L ratio = 10 g/L, and contact time of 800 min. The achieved sorption capacity of the sulfur-impregnated zeolite (1.02 mmol/g) was compared with the parent sample, the natural zeolite (0.28 mmol/g). The results showed that the sorption capacity of SZ increased by 3.6 times, which justifies the modification of zeolites. SEM-EDS and TG-DTG analyses of the Hg(II)-saturated SZ, as well as measuring the amount of exchangeable cations after saturation, served to detect the mechanism of Hg(II) sorption on SZ. The results showed that the combination of sorption mechanisms was responsible for the improved sorption capacity and includes electrostatic attraction, ion exchange, and surface complexation, accompanied by co-precipitation in the form of HgS. The leaching test revealed that the SZ sample has a good capability to retain Hg(II) in its structure in a wide pH range. Taking all the above findings into account, and in particular the significant removal efficiency over a wide concentration range, makes SZ a promising sorbent for environmental application in the remediation of mercury-contaminated sites.

Supplementary Materials: The following are available online at https://www.mdpi.com/2227-9717/9/2/217/s1: Figure S1: SEM secondary electron image of SZ at a magnification of 600×; Figure S2: Distribution of Hg(II) species as a function of pH.

Author Contributions: Conceptualization, investigation, methodology, formal analysis, and writing—original draft preparation: M.U.; SEM-EDS analysis: M.G.; FTIR analysis: A.D.; and writing—review and editing: M.U., M.G., A.D., and I.N. All authors have read and agreed to the published version of the manuscript.

Funding: This work was supported by the bilateral Croatian-Slovenian project Natural Modified Sorbents as Materials for Remediation of Mercury Contaminated Environment (2020–2023), founded by the Croatian Ministry of Science and Education and Slovenian Research Agency (ARRS) and by the Slovenian Research Agency (ARRS) in the framework of the research program Groundwater and Geochemistry (P1-0020).

Institutional Review Board Statement: Not applicable.

Informed Consent Statement: Not applicable.

Data Availability Statement: The data presented in this study will be available on request from the corresponding author.

Acknowledgments: The authors would like to thank Jovica Stojanović for performing XRPD analyses and Milica Spasojević and Snežana Zildžović for performing zeta potential determination and chemical analyses.

Conflicts of Interest: The authors declare no conflict of interest.

References

1. Hay, R.L.; Sheppard, R.A. Occurrence of zeolites in Sedimentary Rocks: An Overview: Occurrence, properties, application. In *Natural Zeolites: Occurrence, Properties, Applications*; Bish, D.L., Ming, D.W., Eds.; Virginia Polytechnic Institute & State University: Blacksburg, VA, USA, 2001; Volume 45, pp. 217–234. [CrossRef]
2. Sheppard, R.A.; Hay, R.L. Formation of zeolites in Open Hydrologic Systems: Occurrence, properties, application. In *Natural Zeolites: Occurrence, Properties, Applications*; Bish, D.L., Ming, D.W., Eds.; Virginia Polytechnic Institute & State University: Blacksburg, VA, USA, 2001; Volume 45, pp. 261–275. [CrossRef]
3. Margeta, K.; Zabukovec Logar, N.; Šiljeg, M.; Farkaš, M. Natural Zeolites in Water Treatment–How Effective is Their Use. In *Water Treatment*; Elshorbagy, W., Chowdhury, R.K., Eds.; IntechOpen: London, UK, 2013; pp. 81–112. [CrossRef]
4. Ordonez, S.; Diaz, E. Basic Zeolites: Structure, Preparation and Environmental Applications. In *Handbook of Zeolites: Structure, Properties and Applications*; Wong, T.W., Ed.; Nova Science Publishers, Inc.: London, UK, 2009; pp. 51–61.
5. Busca, G. Acidity and basicity of zeolites. A fundamental approach. *Microporous Mesoporous Mater.* **2017**, *254*, 3–16. [CrossRef]

6. Verdoliva, V.; Saviano, M.; De Luca, S. Zeolites as Acid/basic Solid Catalysts: Recent Synthetic Developments. *Catalysts* **2019**, *9*, 248. [CrossRef]
7. Carotenuto, G. Electrical Investigation of the Mechanism of Water Adsorption/Desorption by Natural Clinoptilolite Desiccant Used in Food Preservation. *Mater. Proc.* **2020**, *2*, 15. [CrossRef]
8. Diaby, S. Effect of Water Adsorption on Cation-Surface Interaction Energy in the Na-Mordenite of 5.5:1 Si/Al Ratio. *J. Chem.* **2016**, *2016*, 1–9. [CrossRef]
9. Fischer, M. Structure and bonding of water molecules in zeolite hosts: Benchmarking plane-wave DFT against crystal structure dana. *Z. Krist.* **2015**, *230*, 325–336. [CrossRef]
10. Wang, S.; Peng, Y. Natural zeolites as effective adsorbents in water and wastewater treatment. *Chem. Eng. J.* **2010**, *156*, 11–24. [CrossRef]
11. Misealidis, P. Application of natural zeolites in environmental remediation: A short review. *Micropous Mesoporous Mater.* **2011**, *144*, 15–18. [CrossRef]
12. Bjørklund, G.; Dadar, M.; Mutter, J.; Aaseth, J. The toxicology of mercury: Current research and emerging trends. *Environ. Res.* **2017**, *159*, 545–554. [CrossRef]
13. Yokoyama, H. Lecture on Methylmercury Poisoning in Minamata (MPM). In *Mercury Pollution in Minamata*; Springer Briefs in Environmental Science; Springer: Singapore, 2018; pp. 5–51. [CrossRef]
14. Pillay, K.; Cukrowska, E.M.; Coville, N.J. Improved uptake of mercury by sulphur-containing carbon nanotubes. *Microchem. J.* **2013**, *108*, 124–130. [CrossRef]
15. Xu, J.; Garcia Bravo, A.; Lagerkvist, A.; Bertilsson, S.; Sjöblom, R.; Kumpiene, J. Sources and remediation techniques for mercury contaminated soil, review. *Environ. Int.* **2015**, *74*, 42–53. [CrossRef]
16. Wang, J.; Feng, X.; Anderson, C.W.N.; Xing, Y.; Shang, L. Remediation of mercury contaminated sites—A review. *J. Hazard. Mater.* **2012**, *221–222*, 1–18. [CrossRef]
17. Wang, L.; Hou, D.; Cao, Y.; Sik Ok, Y.; Tack, F.M.G.; Rinklebe, J.; O'Connor, D. Remediation of mercury contaminated soil, water, and air: A review of emerging materials and innovative technologies. *Environ. Int.* **2020**, *134*, 105281–105300. [CrossRef]
18. Wajima, T.; Sugawara, K. Adsorption behaviors of mercury from aqueous solution using sulfur-impregnated adsorbent developed from coal. *Fuel Process. Technol.* **2011**, *92*, 1322–1327. [CrossRef]
19. Silva, H.S.; Ruiz, S.V.; Granados, D.L.; Santángelo, J.M. Adsorption of Mercury (II) from Liquid Solutions Modified Activated Carbons. *Mater. Res.* **2010**, *13*, 129–134. [CrossRef]
20. Al-Ghouti, M.; Da'ana, D.; Abu-Dieyeh, M.; Khraisheh, M. Adsorptive removal of mercury from water by adsorbents derived from daze pits. *Sci. Rep.* **2019**, *9*, 15327–15340. [CrossRef]
21. Gupta, A.; Vidyarthi, S.R. Enhanced sorption of mercury from compact fluorescent bulbs and contaminated water streams using functionalized multiwalled carbon nanotubes. *J. Hazard. Mater.* **2014**, *275*, 132–144. [CrossRef]
22. Liu, W.; Zhou, Y.; Hua, Y.; Peng, B.; Deng, M.; Yan, N.; Qu, Z. A sulfur-resistant CuS-modified active coke for mercury removal from municipal solid waste incineration flue gas. *Environ. Sci. Pollut. Res.* **2019**, *26*, 24831–24839. [CrossRef]
23. Tan, G.; Xu, N.; Xu, Y.; Wang, H.; Sun, W. Sorption of mercury (II) and atrazine by biochar, modified biochars and biochar based activated carbon in aqueous solution. *Bioresour. Technol.* **2016**, *211*, 727–735. [CrossRef]
24. Yuan, C.-S.; Lin, H.-Y.; Wu, C.-H.; Liu, M.-H.; Hung, C.-H. Preparation of Sulfurized Powdered Activated Carbon from Waste Tires Using an Innovative Compositive Impregnation Process. *J. Air Waste Manag. Assoc.* **2004**, *54*, 862–870. [CrossRef]
25. Hu, X.; Xue, Y.; Liu, L.; Zeng, Y.; Long, L. Preparation and characterization of Na_2S-modified biochar for nickel removal. *Environ. Sci. Pollut. Res.* **2018**, *25*, 9887–9895. [CrossRef]
26. Abdelouahab-Reddam, Z.; Wahby, A.; El Mail, R.; Silvestre-Albero1, J.; Rodríguez-Reinoso, R.; Sepúlveda-Escribano, A. Activated Carbons Impregnated with Na_2S and H_2SO_4: Texture, Surface Chemistry and Application to Mercury Removal from Aqueous Solutions. *Adsorpt. Sci. Technol.* **2014**, *32*, 101–115. [CrossRef]
27. Cai, J.H.; Jia, C.Q. Mercury Removal from Aqueous Solution Using Coke-Derived Sulfur-Impregnated Activated Carbons. *Ind. Eng. Chem. Res.* **2010**, *49*, 2716–2721. [CrossRef]
28. Asasian, N.; Kaghazchi, T. Sulfurized activated carbons and their mercury adsorption/desorption behavior in aqueous phase. *Int. J. Environ. Sci. Technol.* **2015**, *12*, 2511–2522. [CrossRef]
29. Gebremedhin-Haile, T.; Olguín, M.T.; Solache-Ríos, M. Removal of mercury ions from mixed aqueous metal solutions by natural and modified zeolitic minerals. *Water Air Soil Pollut.* **2003**, *148*, 179–200. [CrossRef]
30. Min, H.-K.; Ahmad, T.; Kim, K.-Y.; Oh, K.-J.; Lee, S.-S. Mercury Adsorption Characteristics of Sulphur-Impregnated Activated Carbon Pellets for the Flue Gas Condition of a Cement-Manufacturing Process. *Adsorpt. Sci. Technol.* **2015**, *33*, 251–262. [CrossRef]
31. Bhatnagar, A.; Hogland, W.; Marques, M.; Sillanpää, M. An overview of the modification methods of activated carbon for its water treatment applications. *Chem. Eng. J.* **2013**, *219*, 499–511. [CrossRef]
32. Xia, M.; Chen, Z.; Li, Y.; Li, C.; Ahmad, N.M.; Cheema, W.A.; Zhu, S. Removal of Hg(II) in aqueous solutions through physical and chemical adsorption principles. *RSC Adv.* **2019**, *9*, 20941–20953. [CrossRef]
33. Perego, C.; Bagatin, R.; Tagliabue, M.; Vignola, V. Zeolites and related mesoporous materials for multi-talented environmental solutions. *Microporous Mesoporous Mater.* **2013**, *166*, 37–49. [CrossRef]
34. *Particle Size Analysis-Sieving Analysis-Part 2: Procedure*; DIN 66165-2; Deutsches Institut für Normung: Berlin, Germany, 2016.

35. Liu, Y.; Khan, A.; Wang, Z.; Chen, Y.; Zhu, S.; Sun, T.; Liang, D.; Yu, H. Upcycling of Electroplating Sludge to Prepare Erdite-Bearing Nanorods for the Adsorption of Heavy Metals from Electroplating Wastewater Effluent. *Water* **2020**, *12*, 1027. [CrossRef]
36. Voinovitch, I.; Debrad-Guedon, J.; Louvrier, J. *The Analysis of Silicates*; Israel Program for Scientific Translations: Jerusalem, Israel, 1966; pp. 127–129.
37. Bohem, H.P. Some aspects of the surface chemistry of carbon blacks and other carbons. *Carbon* **1994**, *32*, 759–769. [CrossRef]
38. US EPA. *Cation-Exchange Capacity of Soils (Ammonium Acetate): Test Methods for Evaluating Solid Waste. SW-846, Method 9080*; US EPA, Office of Solid Waste and Emergency Response: Washington, DC, USA, 1986.
39. Ievtifieieva, O.A.; Bolotov, V.V.; Kostina, T.A.; Svechnikova, O.M.; Yuschenko, T.I.; Kaminska, N.I.; Kosareva, A.E.; Slobodyanyuk, L.V.; Yashchuk, O.P. *Analytical Chemistry (Qualitative Analysis) Part I*; Ievtifieieva, O.A., Ed.; Publishing House the CLL Generous Farmstead Plus: Kharkiv, Ukraina, 2014; pp. 120–121. Available online: https://www.researchgate.net/publication/301527607_Analytical_chemistry_Qualitative_analysis_Part_I_The_manual_for_students_of_higher_schools_O_A_Ievtifieieva_V_V_Bolotov_T_A_Kostina_O_M_Svechnikova_T_I_Yuschenko_N_I_Kaminska_A_E_Kosareva_L_V_Slobodya (accessed on 30 December 2020).
40. Ugrina, M.; Čeru, T.; Nuić, I.; Trgo, M. Comparative Study of Mercury(II) Removal from Aqueous Solutions onto Natural and Iron-Modified Clinoptilolite Rich Zeolite. *Processes* **2020**, *8*, 1523. [CrossRef]
41. German Standard Procedure for Water, Wastewater and Sediment Testing–Sludge and Sediment. *Determination of Leachability*; DIN 38414 S4; Institut für Normung: Berlin, Germany, 1984.
42. Minceva, M.; Fajagar, R.; Markovska, L.; Meshko, V. Comparative study of Zn^{2+}, Cd^{2+}, and Pb^{2+} removal from water solution using natural clinoptilolitic zeolite and commercial granulated activated carbon. Equilibrium and adsorption. *Sep. Sci. Technol.* **2008**, *43*, 2117–2143. [CrossRef]
43. Holleman, A.F.; Wiberg, E. *Inorganic Chemistry*; Academic Press: New York, NY, USA, 2001; pp. 1451–1452.
44. Mozgawa, W. The influence of some heavy metals cations on the FTIR spectra of zeolites. *J. Mol. Struct.* **2000**, *555*, 299–304. [CrossRef]
45. Cadiş, A.-I.; Perhaiţa, I.; Munteanu, V.; Barbu-Tudoran, L.; Silipas, D.T.; Mureşan, L.E. Influence of preparative conditions for obtaining ZnS:Mn nanoparticles using ultrasound-assisted precipitation. *Colloid. Polym. Sci.* **2017**, *295*, 2337–2349. [CrossRef]
46. Hadavifar, M.; Bahramifar, N.; Younesi, H.; Li, Q. Adsorption of mercury ions from synthetic and real wastewater aqueous solution by functionalized multi-walled carbon nanotube with both amino and thiolated groups. *Chem. Eng. J.* **2014**, *237*, 217–228. [CrossRef]
47. Hu, H.; Lin, C.; Zhang, Y.; Cai, X.; Huang, Z.; Chen, C.; Qin, Y.; Liang, J. Preparation of a Stable Nanoscale Manganese Residue-Derived FeS@Starch-Derived Carbon Composite for the Adsorption of Safranine T. *Nanomaterials* **2019**, *9*, 839. [CrossRef]
48. Liu, L.; Zhao, G.H.; Gao, Q.Q.; Chen, Y.J.; Chen, Z.P.; Xu, Z.S.; Li, W.D. Changes of mineralogical characteristics and osteoblast activities of raw and processed pyrites. *RSC Adv.* **2017**, *7*, 28373–28382. [CrossRef]
49. Song, Z.; Zhang, M.; Ma, C. Study on the oxidation of calcium sulfide using TGA and FTIR. *Fuel Process. Technol.* **2007**, *88*, 569–575. [CrossRef]
50. Mozgawa, W.; Król, M.; Barczyk, K. FT-IR studies of zeolites from different structural groups. *CHEMIK* **2011**, *65*, 667–674.
51. Santona, L.; Cozza, C.; Giuliano, V.; Abbruzzese, C.; Nastro, V.; Melis, P. Thermal and spectroscopic studies of zeolites exchanged with metal cations. *J. Mol. Struct.* **2005**, *734*, 99–105. [CrossRef]
52. Nazarenko, V.A.; Antonovich, V.P.; Nevskaja, E.M. *Metal Ions Hydrolysis in Dilute Solutions*; Atomizad: Moscow, Russia, 1979; pp. 34–47.
53. Nies, D.H. The biological chemistry of the transition metal "transportome" of Cupriavidus metallidurans. *Metallomics* **2016**, *8*, 481–507. [CrossRef] [PubMed]
54. Blais, J.F.; Djedidi, Z.; Ben Cheikh, R.; Tyagi, R.D.; Mercier, G. Metals Precipitation from Effluents: Review. *Pract. Period. Hazard. Toxic Radioact. Waste Manag.* **2008**, *12*, 135–149. [CrossRef]
55. Praus, P.; Motáková, M.; Ritz, M. Montmorillonite ion exchanged by mercury (II). *Acta Geodyn. Geomater.* **2012**, *9*, 63–70.
56. Brigatti, M.F.; Colonna, S.; Malferrari, D.; Medici, L.; Poppi, L. Mercury adsorption by montmorillonite and vermiculite: A combined XRD, TG-MS, and EXAFS study. *Appl. Clay Sci.* **2005**, *28*, 1–8. [CrossRef]
57. Rumayor, M.; Diaz-Somoano, M.; Lopez-Anton, M.A.; Martinez-Tarazona, M.R. Mercury compounds characterization by thermal desorption. *Talanta* **2013**, *114*, 318–322. [CrossRef]
58. Li, H.; Dong, X.; da Silva, E.B.; de Oliveira, L.M.; Chen, Y.; Ma, L.Q. Mechanisms of metal sorption by biochars: Biochar characteristics and modifications. *Chemosphere* **2017**, *178*, 466–478. [CrossRef]
59. Gong, Y.; Liu, Y.; Xiong, Z.; Zhao, D. Immobilization of Mercury by Carboxymethyl Cellulose Stabilized Iron Sulfide Nanoparticles: Reaction Mechanisms and Effects of Stabilizer and Water Chemistry. *Environ. Sci. Technol.* **2014**, *48*, 3986–3994. [CrossRef]
60. Zhang, S.; Zhang, X.; Xiong, Y.; Wang, G.; Zheng, N. Effective solidification/stabilisation of mercury-contaminated wastes using zeolites and chemically bonded phosphate ceramics. *Waste Manag. Res.* **2015**, *33*, 183–190. [CrossRef]
61. Shi, J. The Applications of Zeolite in Sustainable Binders for Soil Stabilization. *Appl. Mech. Mater.* **2013**, *256–259*, 112–115. [CrossRef]
62. Mola-Abasi, H.; Kordtabar, B.; Kordnaeij, A. Effect of Natural Zeolite and Cement Additive on the Strength of Sand. *Geotech. Geol. Eng.* **2016**, *34*, 1539–1551. [CrossRef]